

1
2 **Distributed summer air temperatures across mountain glaciers:**
3 **climatic in the south-east Tibetan Plateau: temperature sensitivity and**
4 **comparison with existing glacier sizedatasets**
5

6 Thomas E. Shaw¹, Wei Yang^{2,3}, Álvaro Ayala⁴, Claudio Bravo⁵, Chuanxi Zhao², Francesca
7 ~~Pellicciotti~~^{6,7}Pellicciotti^{1,6}
8

9 ⁴~~Advanced Mining Technology Center, Universidad de Chile, Santiago, Chile~~

10 ¹~~Federal Institute for Forest, Snow and Landscape Research (WSL), Birmensdorf, Switzerland~~

11 ² Key Laboratory of Tibetan Environment Changes and Land Surface Processes, Institute of
12 Tibetan Plateau Research, Chinese Academy of Sciences (CAS), Beijing, China

13 ³ CAS Center for Excellence in Tibetan Plateau Earth Sciences, Beijing 100101, China

14 ⁴ Centre for Advanced Studies in Arid Zones (CEAZA), La Serena, Chile

15 ⁵ School of Geography, University of Leeds, Leeds, UK

16 ⁶~~Federal Institute for Forest, Snow and Landscape Research (WSL), Birmensdorf, Switzerland~~

17 ⁷6 Department of Geography, Northumbria University, Newcastle, UK
18

19 *Corresponding author: Thomas E. Shaw (thomas.shaw@amtc.uchile.ch)*
20

21 Keywords: Air Temperature, Glaciers, Tibetan Plateau, ~~Climatic Sensitivity~~temperature
22 sensitivity
23

24 **Abstract**

25 Near-surface air temperature (T_a) is highly important for modelling glacier ablation, though its
26 spatio-temporal variability over melting glaciers still remains largely unknown. We present a new
27 dataset of distributed T_a for three glaciers of different size in the south-east Tibetan Plateau during
28 two monsoon-dominated summer seasons. We compare on-glacier T_a to ambient T_a extrapolated
29 from several, local off-glacier stations. We parameterise the along-flowline ~~climatic~~-sensitivity of
30 T_a on these glaciers to changes in off-glacier temperatures (referred to as temperature sensitivity)
31 and present the results in the context of ~~several~~-available distributed on-glacier datasets around
32 the world. ~~Climatic~~Temperature sensitivity decreases rapidly up to 2000-3000 m along the down-
33 glacier flowline distance. Beyond this distance, both the T_a ~~of~~on the Tibetan glaciers and global
34 glacier datasets show ~~a slower decrease of climatic sensitivity, little additional cooling relative to~~
35 the off-glacier temperature. In general, ~~observations~~ T_a on small glaciers (with ~~<1000 m~~-flowline
36 ~~distance~~) are~~distances < 1000 m~~ is highly sensitive to temperature changes outside the glacier
37 boundary layer. The climatology of a given region can influence the general magnitude of this
38 ~~climatic~~temperature sensitivity, though no strong relationships are found between along-flowline
39 ~~climatic~~temperature sensitivity and mean summer temperatures or precipitation. The terminus of
40 some glaciers ~~remain associated with~~are affected by other warm air processes that increase
41 ~~climatic~~temperature sensitivity (such as divergent boundary layer flow, warm up-valley winds or
42 debris/valley heating effects) which are evident only beyond ~70% of the total glacier flowline
43 distance. Our results therefore suggest a strong role of local effects in modulating
44 ~~climatic~~temperature sensitivity close to the glacier terminus, although further work is still
45 required to explain the ~~variable presence~~variability of these effects for different glaciers.
46

47 **1. Introduction**

48 Near-surface air temperature (T_a) is one of the dominant controls on glacier energy and mass
49 balance during the ablation season (Petersen et al., 2013; Gabbi et al., 2014; Sauter and Galos,
50 2016; Maurer et al., 2019; Wang et al., 2019), though modelling its spatio-temporal behaviour
51 above melting ice surfaces remains a challenge. The absence of distributed information regarding
52 T_a has favoured the use of simple, space-time invariant relationships of T_a with elevation, typically
53 that of the free-air environmental lapse rate (ELR). ~~The physical processes of the~~ free-air (that
54 ~~which is independent of the ELR cannot be reliably used to estimate near-surface boundary layer);~~
55 ~~however, are not appropriate to describe the variability of T_a for local glacier boundary layers~~
56 ~~(Figure 1a), especially when the air temperatures above ice temperature gradient (melting~~
57 ~~glaciers, where steep gradients are found within ~10 m of the ice surface) heightens under warm~~
58 ‘ambient’ (off-glacier) conditions (van den Broeke, 1997; Greuell and Böhm, 1998; Oerlemans,
59 2001; Oerlemans and Grisogono, 2002; Ayala et al., 2015). As a result, any extrapolation of T_a
60 observations from an off-glacier location, particularly those at lower elevations, are likely to lead
61 to an overestimation of snow and ice ablation in energy balance and enhanced temperature index
62 melt simulations (e.g. Petersen and Pellicciotti, 2011; Pellicciotti et al., 2014; Shaw et al., 2017).
63 While models applying the degree day approach can make use of off-glacier temperatures as
64 forcing because they are heavily reliant on calibration, for energy balance models and models of
65 intermediate complexity (Pellicciotti et al., 2005; Ragetti et al., 2016) it is key to resolve the air
66 temperature distribution over glaciers, especially for turbulent flux calculations ~~Whilst this and~~
67 typical parameterizations of incoming longwave radiation.

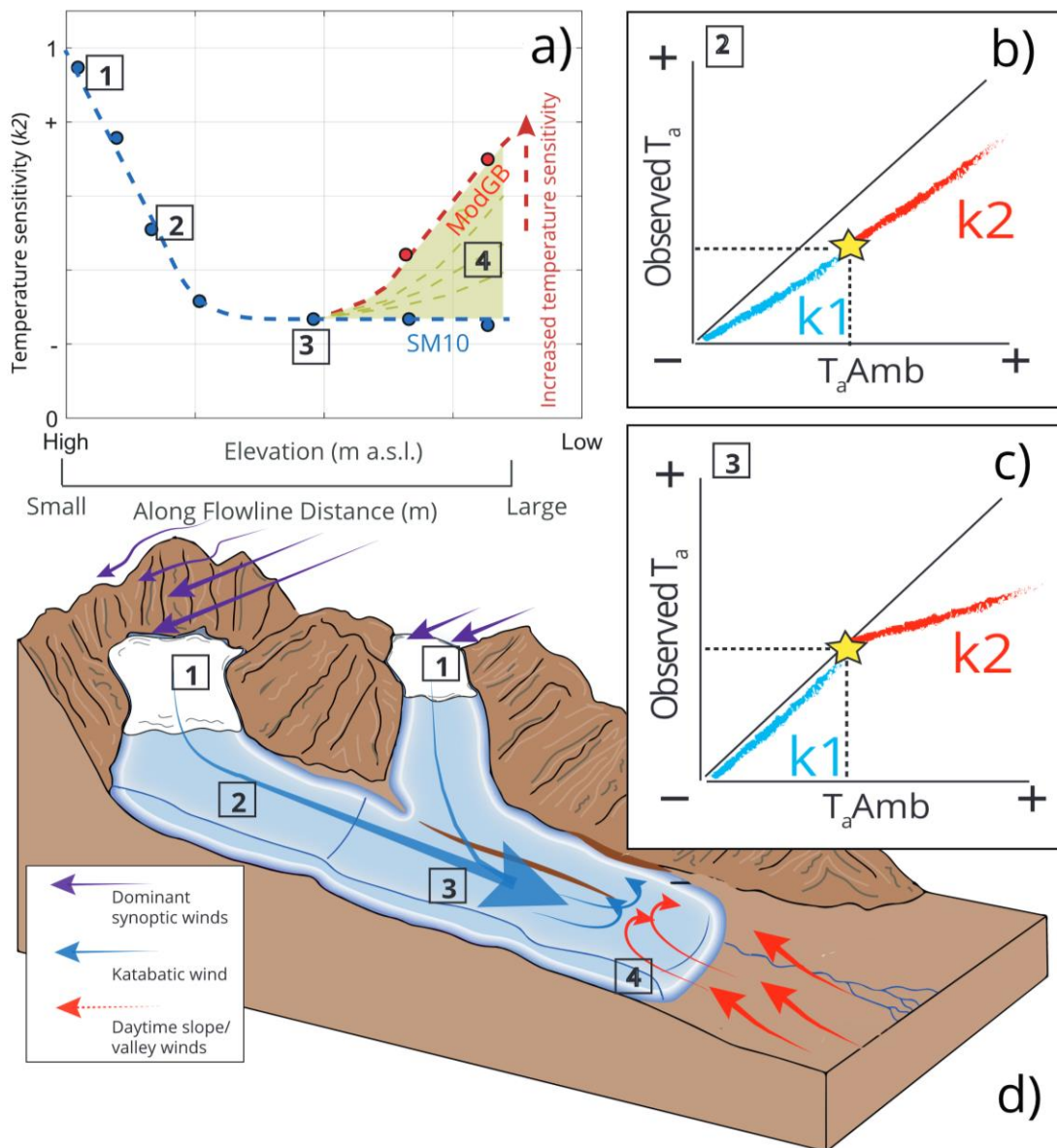
68
69 This problem has been long understood (Greuell et al., 1997; Greuell and Böhm, 1998), but only
70 within the last decade have studies approached it in more detail (Petersen et al., 2013; Ayala et
71 al., 2015; Carturan et al., 2015; Shaw et al., 2017; Bravo et al., ~~2019~~2019a; Troxler et al., 2020).
72 Until recently, modelling studies have relied upon simple lapse rates (including the ELR) and/or
73 single bias offset values to account for the ‘cooling effect’ of the near-surface air on-glacier
74 (Arnold et al., 2006; Nolin et al., 2010; Ragetti et al., 2016). The variations of T_a along the glacier
75 flowline (defined following Shea and Moore (2010) as the horizontal distance from an upslope
76 summit or ridge), however, are much more complex (Ayala et al., 2015; Shaw et al., 2017), though
77 a lack of available data usually restricts one’s ability to appropriately model this variable. ~~While~~
78 ~~models applying the degree day approach can make use of off-glacier temperatures as forcing~~
79 ~~because they are heavily reliant on calibration, for physically based models and models of~~
80 ~~intermediate complexity (Pellicciotti et al., 2005; Ragetti et al., 2016) it is key to resolve the air~~
81 ~~temperature distribution over glaciers, especially for turbulent flux calculations.~~

82
83 To date, two main, simplified model approaches have been developed and tested to represent air
84 temperature over glaciers (Figure 1a). The first is the statistical model by Shea and Moore (2010)
85 developed to reconstruct T_a across glaciers of varying size in ~~the Canadian Rockies~~western
86 Canada from ambient temperature records. This approach considered the ratios of observed
87 on-glacier temperature and estimated ambient temperature for the elevation of a given point on a
88 glacier (hereafter ‘ $T_{a,Amb}$ ’). The authors calculated two ratios from a piecewise regression above
89 and below a critical threshold temperature for the onset of the glacier katabatic boundary layer
90 (KBL). - see section 4.3). The parameterisations that operate as a function of the along-flowline
91 distance have since been explored tested by Carturan et al. (2015) and Shaw et al. (2017) on
92 smaller glaciers in different parts of the Italian Alps. Carturan et al. (2015) found that the original
93 published parameterisations were sufficient to explain T_a on small, fragmenting glaciers up to
94 flowline distances of ~2000m. However, investigation by Shaw et al. (2017) on a small alpine
95 glacier found a pattern of along-flowline T_a that was better described by an alternative,
96 thermodynamic model approach. This second, physically-oriented approach was developed by
97 Ayala et al. ~~(2015) based upon modifications of the original model by Greuell and Böhm~~
98 ~~(1998)~~(2015) to account for a relative ‘warming effect’ evident on the termini of some mountain
99 glaciers when compared to upper elevations ~~that were fully dominated by katabatic winds~~. The
100 modified model (termed ‘ModGB’ in the literature) accounts for the down-glacier cooling of T_a
101 at increasing flowline distances due to sensible heat exchange and adiabatic heating (Greuell and
102 Böhm, 1998). It adds, ~~however, an additional~~ a warming factor based upon on-glacier

103 observations in the lower sections of the glacier (e.g. at the greatest flowline distances) to account
104 for additional processes of adiabatic warming (Ayala et al., 2015) (Figure 1a). The ModGB
105 approach has been successively applied at other glacier sites around the world (Shaw et al., 2017;
106 Troxler et al., 2020), though the question of its transferability remains open (Troxler et al., 2020).

107
108 ~~Thus~~In this way, the ModGB method operates on the physical principles of the glacier boundary
109 layer (Greuell and Böhm, 1998) though it corrects for relative warming on the lower portion of
110 glacier (Ayala et al., 2015). To establish the magnitude of this warming, however, along-flowline
111 data in the lower portion of the glacier are essential. Because the available distribution of on-
112 glacier observations is often limited and rarely extends for the entire length of the glacier
113 ~~boundary layer~~flowline, this additional correction for warming ~~and associated with~~ the ~~number of~~
114 ~~physical unknowns~~unknown parameters of ModGB can lead to high variability in T_a estimates on
115 the lower glacier ~~terminus~~ablation zone (Troxler et al., 2020) (Figure 1a). In contrast to this, the
116 statistical method of Shea and Moore (2010) provides a more simplified estimation that has fewer
117 assumptions and parameters, though it does not explicitly account for ~~the~~ physical processes ~~on~~
118 ~~the glacier, especially those that are~~ thought to be the cause of ‘relative warming for warming’ on
119 the glacier terminus. It also provides a parameter that more specificallyexplicitly represents the
120 glacier ‘climatic temperature sensitivity’ of the on-glacier T_a (defined here as the ratio of changes
121 in observed T_a on-glacier to changes in T_{aAmb}). ~~- Figure 1b and 1c~~. Despite its more conceptual
122 nature, because of its greater generalisabilityease of applicability, typical of a more simplistic
123 statistical approach, we adopt the Shea and Moore (2010) method to further investigate along-
124 flowline T_a in this study.

125
126 ~~To the author's knowledge, no study has investigated the variability of on-glacier T_a at different~~
127 ~~sites around the world (with the exception of three glaciers considered by Ayala et al., (2015)).~~



129

130

131

132

133

134

135

136

137

138

139

140

141

142

143

144

145

146

147

Figure 1: A schematic diagram to describe the temperature sensitivity of on-glacier air temperature (T_g) to the extrapolated ambient temperature ($T_{a,amb}$) at given elevations/flowline distances on a mountain glacier. Points 1-4 indicate locations of interest that are linked between panels. Panel (a) indicates the along-flowline 'k2' temperature sensitivities to $T_{a,amb}$, considering the differences represented by the models of SM10 and ModGB for glacier termini (see text). Panels (b) and (c) represent the differences of k_1 (blue) and k_2 (red) sensitivities observed in the data at different theoretical locations on the glacier, the latter of which shows the theoretical parameterisation presented by Shea and Moore (2010). The yellow stars indicate the calculated threshold for katabatic onset (T^ in the text). Panel (d) represents an idealised case of katabatic and valley/synoptic wind interactions that potentially dictate the along-flowline structure of on-glacier temperature sensitivity and thus T_g estimation.*

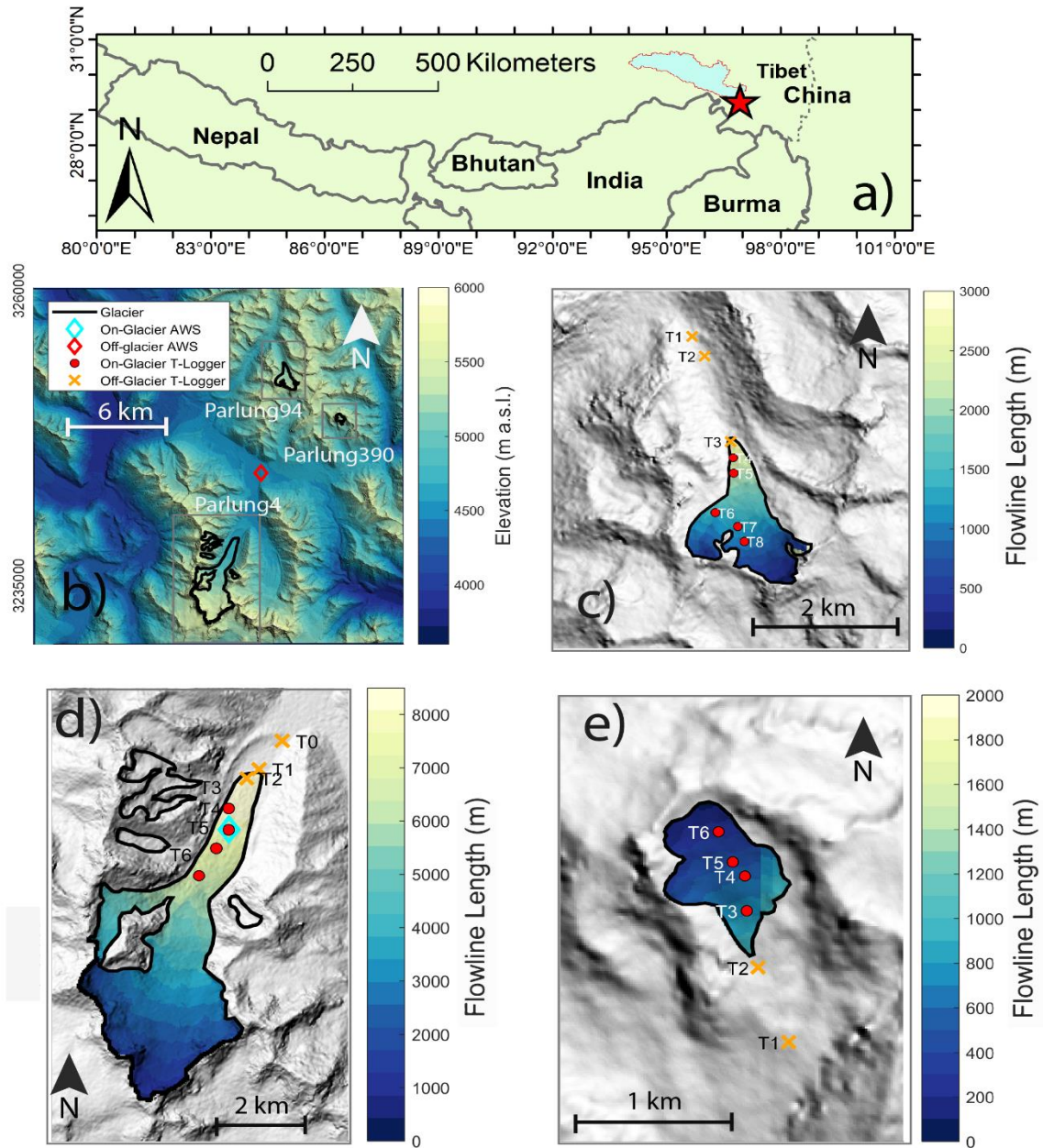
To date, few studies have investigated the variability of distributed, on-glacier T_g at different sites around the world. As such, the transferability of temperature estimation models and/or model parameters remain mostly unknown, and analysis of individual glacier sites, while beneficial to process understanding, may not advance the science on how to treat the on-glacier T_g in models. In this study, we ~~make a step toward this by utilising~~ use new datasets of on-glacier temperature observations on three glaciers of varying size in the south-east Tibetan Plateau. We

148 analyse the main controls on along-flowline T_a and its ~~climatic~~ temperature sensitivity and present
149 these new findings in the context of 11 other ~~distributed~~ on-glacier observations around the world
150 ~~made to date~~.

151 Specifically we aim to i) understand the variability of T_a with the along-flowline distances at three
152 glaciers in the south-east Tibetan Plateau, ii) identify and quantify the ~~climatic~~ temperature
153 sensitivity of on-glacier T_a for different meteorological conditions and glacier sizes and iii)
154 parameterise the along-flowline T_a using the Shea and Moore (2010) method for the Tibetan
155 glaciers and discuss it in the context of globally-derived, published datasets of on-glacier air
156 temperatures.

158 2. Study Site

159 The study glaciers are located in the upper Parlung-Zangbo River catchment in the southeast Tibet
160 Plateau (29.24°N, 96.93°E - Figure 2), a region characterised by a summer monsoon climate that
161 typically intrudes via the Brahmaputra Valley (Yang et al., 2011). We present data for three
162 maritime-type valley glaciers in the ~~wider~~ Parlung-Zangbo catchment: Parlung Glacier Number
163 4 (hereafter ‘Parlung4’), Parlung Glacier Number 94 (‘Parlung94’) and Parlung Glacier Number
164 390 (‘Parlung390’). Parlung4 (Figure 2d) is ~10.8 km², north-northeast facing and has an
165 elevation range of 4659-5939 m a.s.l. (Ding et al., 2017). Glaciers Parlung94 (Figure 2c) and
166 Parlung390 (Figure 2e) are smaller valley glaciers (2.51 and 0.37 km², respectively) that have
167 termini at higher elevations (elevation ranges of 5000-5635 and 5195-5469 m a.s.l.,
168 respectively). The glaciers of the catchment were classified by Yang et al. (2013) as having a
169 spring-accumulation regime and the ~~largest annual~~ longest rain season of the entire Tibetan
170 Plateau. The upper Parlung River catchment has a mean summer (1979-2019) annual air
171 temperature of ~2°C (at 4600 m a.s.l.), and temperatures in the wider region have been shown to
172 be increasing since the mid 1990’s (Yang et al., 2013). The glaciers of this region have been
173 shown to be very sensitive to temperature changes, though with a ~~more elevation independent~~
174 ~~lower sensitivity of~~ mass balance ~~sensitivity to elevation~~ compared to other, continental glaciers
175 of the Tibetan Plateau (Wang et al., 2019). ~~The~~ ~~Because Tibetan glaciers are shrinking and~~
176 ~~fragmenting, the~~ accurate estimation of on-glacier temperatures ~~as Tibetan glaciers shrink and~~
177 ~~fragment is relevant for investigating and modelling their temperature sensitivity~~ (Carturan et al.,
178 2015) ~~is thus of significant importance for continued modelling efforts.~~ However, to date, no
179 ~~such~~ studies regarding ~~the distribution of~~ on-glacier temperature ~~distribution~~ have ~~been~~ performed
180 within the Tibetan Plateau.



182
 183 *Figure 2: The location of Parlung catchment in Tibet (a) and a map of the Parlung glaciers (b) with the*
 184 *study glaciers, Parlung 94 (c), Parlung4 (d) and Parlung390 (e). Off-glacier and on-glacier AWS and T-*
 185 *Logger locations are shown (without glacier number suffix - see Table 1). (b) shows the elevation of the*
 186 *catchment (DEM source: Alos Palsar) and (c-e) show the calculated flowline distances based upon*
 187 *TopoToolbox (scales vary).*

188
 189

190 3. Data

191 3.1. *Air temperature* *Meteorological* observations

192 We present the observations of T_a from a total of 20 air temperature logger locations (Table 1),
 193 13 of which are situated on-glacier (4680 - 5369 m a.s.l.) and seven off-glacier (4648 - 5168 m
 194 a.s.l.). These stations (hereafter referred to as ‘T-loggers’) observed T_a at a 2 m height using
 195 HOBO U23-001 temperature-relative humidity sensors (accuracy $\pm 0.21^\circ\text{C}$) within double-
 196 louvered, naturally-ventilated radiation shields (**HOBO RS1**) mounted on free-standing tripods.
 197 The T-loggers recorded data in 10 minute intervals that are averaged to hourly data for analysis.

We identify a common observation period over the summers of 2018 and 2019 that ~~rangeranges~~ from 12th July – 18th September. For these date ranges, we observe only small data gaps for some T-loggers (~~Table~~ ($< 1\%$ of the total period)). We apply the nomenclature of TX_G , whereby X refers to the T-logger number on each glacier and G refers to the glacier number. ~~(Table 1).~~ (Table 1).

Table 1: Details of each AWS/T-Logger station used in this analysis including the calculated flowline distances.

<u>Station</u>	<u>Latitude</u>	<u>Longitude</u>	<u>Elevation (m a.s.l.)</u>	<u>Flowline (m)</u>	<u>on/off glacier</u>
<u>AWS_Off</u>	<u>29.314</u>	<u>96.955</u>	<u>4588</u>	=	<u>off</u>
<u>AWS_On</u>	<u>29.500</u>	<u>97.009</u>	<u>4808</u>	=	<u>off</u>
<u>T1₃₉₀</u>	<u>29.348</u>	<u>97.022</u>	<u>5095</u>	=	<u>off</u>
<u>T2₃₉₀</u>	<u>29.352</u>	<u>97.020</u>	<u>5168</u>	=	<u>off</u>
<u>T3₃₉₀</u>	<u>29.354</u>	<u>97.0202</u>	<u>5258</u>	<u>770</u>	<u>on</u>
<u>T4₃₉₀</u>	<u>29.356</u>	<u>97.020</u>	<u>5310</u>	<u>544</u>	<u>on</u>
<u>T5₃₉₀</u>	<u>29.357</u>	<u>97.019</u>	<u>5335</u>	<u>420</u>	<u>on</u>
<u>T6₃₉₀</u>	<u>29.359</u>	<u>97.018</u>	<u>5377</u>	<u>224</u>	<u>on</u>
<u>T1₉₄</u>	<u>29.621</u>	<u>97.218</u>	<u>4965</u>	=	<u>off</u>
<u>T2₉₄</u>	<u>29.417</u>	<u>96.99</u>	<u>4992</u>	=	<u>off</u>
<u>T3₉₄</u>	<u>29.635</u>	<u>96.975</u>	<u>5086</u>	=	<u>off</u>
<u>T4₉₄</u>	<u>29.596</u>	<u>97.065</u>	<u>5138</u>	<u>2481</u>	<u>on</u>
<u>T5₉₄</u>	<u>29.56</u>	<u>97.067</u>	<u>5174</u>	<u>2215</u>	<u>on</u>
<u>T6₉₄</u>	<u>29.466</u>	<u>97.023</u>	<u>5302</u>	<u>1411</u>	<u>on</u>
<u>T7₉₄</u>	<u>29.434</u>	<u>97.080</u>	<u>5280</u>	<u>1208</u>	<u>on</u>
<u>T8₉₄</u>	<u>29.399</u>	<u>97.097</u>	<u>5331</u>	<u>988</u>	<u>on</u>
<u>T1₄</u>	<u>29.271</u>	<u>96.968</u>	<u>4690</u>	=	<u>off</u>
<u>T2₄</u>	<u>29.368</u>	<u>96.935</u>	<u>4769</u>	=	<u>off</u>
<u>T3₄</u>	<u>29.298</u>	<u>97.168</u>	<u>4806</u>	<u>8589</u>	<u>on</u>
<u>T4₄</u>	<u>29.298</u>	<u>97.168</u>	<u>4809</u>	<u>7940</u>	<u>on</u>
<u>T5₄</u>	<u>29.496</u>	<u>97.126</u>	<u>4841</u>	<u>7505</u>	<u>on</u>
<u>T6₄</u>	<u>29.403</u>	<u>97.068</u>	<u>4909</u>	<u>6765</u>	<u>on</u>

We additionally present T_a observations at two automatic weather stations (AWS) at elevations ~4600 m a.s.l. (off-glacier, henceforth ‘AWS_Off’) and ~~~4650~~4800 m a.s.l. (on Parlung4, henceforth ‘AWS_On’) for the same time period (Figure 2). ~~For distributing off glacier air temperature, we consider AWS_Off as our reference station.~~ The AWS T_a observations are provided by Vaisala HMP60 temperature-relative humidity sensors (accuracy $+0.5^\circ\text{C}$) ~~also housed in naturally-ventilated radiation shields.~~ housed in naturally-ventilated, Campbell 41005-5 radiation shields. We obtain information regarding incoming shortwave radiation and relative humidity (AWS_Off), on-glacier wind speed (AWS_On) and ‘free-air’ wind speed and direction (ERA5 - C3S, 2017). We use these data to explore the relationships of hourly on- and off-glacier temperatures (section 4.2) for different prevailing conditions.

3.2. Uncertainty Intercomparison of air temperature observations

222 To ~~provide an estimate~~ evaluate the comparability of ~~observation uncertainty~~ air temperature
223 ~~measurements~~, we ~~compared~~ calculate the hourly divergence of two naturally-ventilated T_a
224 observations for the whole period between T4₄ and AWS_On (Figure 2d), that are ~~co~~-located
225 within a few metres of horizontal distance of each other on Parlung4 Glacier. A test of absolute
226 differences between the two stations resulted in a mean of $< 0.4^\circ\text{C}$ for all hours ($n = 3312$) and
227 $\sim 0.5^\circ\text{C}$ for the warmest 10% of the hours of ambient temperature at AWS_Off. We find that for
228 these warm hours (hereafter referred to as ‘P90’ - (Ayala et al., 2015; Shaw et al., 2017; Troxler
229 et al., 2020)). ~~We find that for these hours (-)~~, when the *KBL* development is theoretically at its
230 strongest (e.g. van den Broeke, 1997; Oerlemans and Grisogono, 2002)), that 95% of hourly
231 differences were $< 1^\circ\text{C}$ (Figure S1). For on-glacier stations at large flowline distances (Figure 2),
232 these large uncertainties differences are considered less likely given the good ventilation provided
233 to the sensors within the *KBL*. While observations at short flowline distances with calm
234 conditions and high incoming radiation may result in ~~maximum uncertainties~~ larger differences
235 up to $\sim 1^\circ\text{C}$ (Troxler et al., 2020), we apply a $\pm 0.5^\circ\text{C}$ ~~uncertainty~~ ‘uncertainty’ for analysis of
236 distributed T_a . For the instantaneous differences $> 1^\circ\text{C}$, wind speeds at AWS_On were $< 2 \text{ m s}^{-1}$.
237 Wind speeds for P90 conditions were otherwise in excess of $3\text{-}4 \text{ m s}^{-1}$, though no other
238 observations of on-glacier wind speed are available at higher elevations. We note that in the
239 absence of an artificially ventilated T_a measurement as a reference (e.g. Georges and Kaser, 2020;
240 Carturan et al., 2015), a true uncertainty value cannot be prescribed for the T_a observations of our
241 study and only assumed based upon previous literature. This is discussed further in section 6.
242

243 3.3. Meteorological information

244 ~~We obtained information regarding T_a , incoming shortwave radiation and relative humidity~~
245 ~~(AWS_Off), on glacier wind speed (AWS_On) and ‘free air’ wind speed and direction (ERA5-~~
246 ~~C3S, 2017). We used these data to explore the relationships of hourly on and off glacier~~
247 ~~temperatures (section 4.2) for different prevailing conditions.~~
248

249 3.4.3.3. Elevation information

250 We ~~used~~ use the 12.5 m Alos Palsar (ASF DAAC, 2020) digital elevation model (DEM) to
251 ~~provide~~ obtain elevation information for the catchment (Figure 2b). ~~We utilised this DEM in order~~
252 ~~to calculate flowline~~ Flowline distances (m) for each glacier are calculated from the TopoToolbox
253 functions in Matlab (Schwanghart and Kuhn, 2010), following Troxler et al, (2020). We note that
254 the methodology for flowline generation is not currently uniform among all studies of this type
255 (Shea and Moore, 2010; Ayala et al., 2015; Carturan et al., 2015; Shaw et al., 2017; Bravo et al.,
256 ~~2019~~2019a; Troxler et al., 2020) and may produce some differences in the calculated distances
257 close to the lateral borders of the glaciers. In addition, the generated flowlines may also be
258 dependent upon the quality and resolution of the DEM available ~~between the aforementioned~~
259 ~~studies.~~ However, we do not analyse lateral T_a variations in this study and consider ~~that~~ the
260 impact of varying methods for flowline generation to be negligible when assessing observations
261 at a few ~~select~~ selected points on the glacier.
262

263 4. Methods

264 ~~For this study we use local, off glacier T_a data from AWS_Off for aggregation~~ Our methods
265 ~~consist of (1) aggregating temperature observations based on glacier sub groups or for~~
266 ~~distribution of T_a in space. Sub grouping allows one to interpret general causal factors that dictate~~
267 ~~on glacier behaviour, whereas the distribution in space allows a direct comparison of on and off-~~
268 ~~glacier temperatures and prevailing meteorological conditions, (2) generating off-glacier~~
269 ~~temperature lapse rates to compare on and off-glacier temperatures at the same elevation, and (3)~~
270 ~~estimating the effect of near-surface temperature sensitivity by fitting parameters to the glacier~~
271 ~~boundary layer model of Shea and Moore (2010). The following subsections outline the sub-~~
272 ~~grouping (4.1) and off-glacier T_a distribution (4.2) methodologies. The model parameterisations~~

273 of Shea and Moore (2010) and application to Tibetan and global datasets are ~~considered~~described
 274 in sections 4.3 and 4.4, respectively.

275 4.1. *Sub-grouping on-glacier air temperature observations*

276 Sub-grouping allows one to interpret general causal factors that dictate on-glacier behaviour. We
 277 sub-group our on-glacier observations by 10th and 90th percentiles (P10 ~~= the coldest 10%~~, P90 ~~= the warmest 10%~~)
 278 of off-glacier T_a at AWS_Off (Figure 2a) ~~that have been shown to relate to~~
 279 ~~the development of the glacier boundary layer (Ayala et al., 2015).~~ Following the methodology
 280 of previous studies (Ayala et al., 2015; Shaw et al., 2017; Troxler et al., 2020), we ~~consider~~bin all
 281 contemporaneous observations of on-glacier T_a at each T-logger that ~~relate~~correspond to the same
 282 hours as the coldest (P10 ~~= the coldest 10%~~) and warmest (P90 ~~= the warmest 10%~~) observations at AWS_Off. We
 283 ~~consider~~evaluate how strong the ~~deviation from a~~ linear relationship of on-glacier T_a with
 284 elevation and flowline distance is for these subgroups, ~~assessing this ‘linearity’ by use of~~ using
 285 the coefficient of determination (R^2). For a comparison to previous studies (Petersen and
 286 Pellicciotti, 2011; Shaw et al., 2017), we also report the equivalent on-glacier lapse rate that would
 287 be calculated for the above conditions.

288 4.2. *Comparison of on- and off-glacier air temperature*

289 We extrapolate AWS_Off T_a records to the elevation of each on-glacier T-logger (Table 1) to
 290 quantify the T_a -differences within the between ambient and on-glacier boundary layer T_a (Figure
 291 1a). We derive an hourly variable lapse rate between AWS_Off and off-glacier ~~T-loggers deemed~~
 292 ~~to be independent of the glacier wind layer, thus excluding those T-loggers in the immediate pro-~~
 293 ~~glacial zones. Specifically, we use AWS_Off and~~ T-loggers T1₉₄, T2₉₄ and T1₃₉₀ to construct a
 294 ‘catchment lapse rate’ where the origin of the calculated regression must pass through the
 295 elevation of AWS_Off ~~that acts as the forcing station in this study~~ (see supplementary
 296 information, Figure S2). ~~We~~ These T-loggers are assumed to be unaffected by the glacier
 297 boundary layer and we consider this as the best available approach to estimate the ambient lapse
 298 rate for the catchment. ~~We~~ compare the hourly estimates of the extrapolated off-glacier T_a
 299 (T_{aAmb}) with the observations at each on-glacier T-logger in order to i) understand how
 300 large quantify the T_a -~~offset (bias) is at each site~~ differences and how it relates they relate to
 301 meteorological conditions and glacier flowline distance; and ii) parameterise the along flowline
 302 ~~elimati~~temperature sensitivity to T_{aAmb} following Shea and Moore (2010) (section 4.3).
 303

304 4.3. *Estimation of on-glacier ~~elimati~~temperature sensitivity*

305 The Shea and Moore (2010) approach (hereafter ‘SM10’) estimates on-glacier T_a using T_{aAmb} at
 306 a given elevation by:
 307
 308

$$309 \quad T_a = \begin{cases} T1 + k2(T_{aAmb} - T^*), & T_{aAmb} \geq T^* \\ T1 - k1(T^* - T_{aAmb}), & T_{aAmb} < T^* \end{cases}$$

$$310 \quad T_a = \begin{cases} T1 + k2(T_{aAmb} - T^*), & T_{aAmb} \geq T^* \\ T1 - k1(T^* - T_{aAmb}), & T_{aAmb} < T^* \end{cases} \quad (1)$$

311
312

313 where T^* (°C) represents the threshold ambient temperature for the onset of katabatic flow and
 314 $T1$ is the corresponding threshold T_a on the glacier. Parameters $k1$ and $k2$ are the
 315 ~~elimati~~temperature sensitivities (ratio of on-glacier T_a to T_{aAmb}) below and above the threshold
 316 T^* (Figure 1b and c). $k1$ and $k2$ were parameterised in the original study using exponential
 317 functions of the along flowline distance (DF):
 318

$$319 \quad k1 = \beta1 \exp(\beta2 DF) \exp \exp(\beta2 DF)$$

320 (2)

$$k2 = \beta3 + \beta4 \exp(\beta5 DF)$$

(3)

where β_i are the fitted coefficients. Following the suggestion of Carturan et al. (2015), we implement a relation against the flowline that estimates the threshold temperature for onset of katabatic effects (T^*) at a given distance as:

$$T^* = \frac{C1DF}{C2 + DF}$$

(4)

where $C1$ (6.61) and $C2$ (436.04) are the fitted coefficients of Carturan et al. (2015). We calculate $k1$ and $k2$ at each T-logger station using the linear regression of observed T_a and T_{aAmb} above and below T^* (Figure 1) as derived from equation 4. We note that the parameter $k2$ holds a greater significance for modelling T_a (Figure 1a), as this more closely represents the ‘climatic sensitivity’ reported by previous works (Greuell et al., 1997; Greuell and Böhm, 1998; Oerlemans, 2001; 2010), whereas $k1$ represents the ratio of above-glacier and free-air temperatures without a katabatic effect that have been shown to relate more closely to T_{aAmb} (Shea and Moore, 2010; Shaw et al., 2017). For this study, we therefore pay particular attention to the $k2$ sensitivities on the Parlung glaciers and assess their relationship to along-flowline distance.

4.3.4. Global datasets of on-glacier temperatures

To explore the generalisability of the SM10 approach and provide context to the findings of the Parlung catchment, we explore the calculated $k1$ and $k2$ parameters for several of the available distributed on-glacier datasets published to date (Figure S3, Table 2). We subset data for each glacier to those hours during the summer periods when all available on-glacier observations were available at a given site. For sites of the Coastal Mountains of British Columbia (‘CMBC’ - Shea and Moore, 2010) and Alta Val de La Mare (‘AVDM’ - Carturan et al., 2015), we apply the published parameter sets derived from those authors. For all other sites, we derive T_{aAmb} from the most locally available off-glacier AWS and the published lapse rate from the relevant studies (Table 2). In the absence of lapse rate information for a few glaciers, we apply the ELR ($-6.5^\circ\text{C km}^{-1}$) to extrapolate T_a to the elevation of the on-glacier observations. (see Table 2). We found that the calculation of $k1$ and $k2$ at those few glacier sites were not sensitive to the choice of lapse rate used, and varied $< \pm 0.03$ for a $\pm 1.5^\circ\text{C km}^{-1}$ change in the lapse rate. For each glacier site, data are limited to those hours when all stations for that glacier are available and, the $k1$ and $k2$ parameters (equation 1) are only calculated when; i), $>10\%$ of the total hourly data at a given station is above or below T^* (to have enough data to calculate $k2$ and $k1$, respectively) and, ii) the linear regression to derive each parameter is significant to the 0.95 level. For those on-glacier stations that do not satisfy the above requirements, we do not calculate the $k1$ and $k2$ parameters.

Table 2: The details of each site where distributed on-glacier air temperatures are available. Elevation ranges and ERA5 mean summer air temperatures (MSAT) are reported for the year of investigation. Precipitation totals (mm – ‘PT’) were obtained from the cited literature.

Site	Lat	Lon	Year(s)	Elevation	MSA T ^a	PT	T _a Data Reference
------	-----	-----	---------	-----------	-----------------------	----	-------------------------------

				<u>m .a.s.l.</u>	<u>°C</u>	<u>mm</u>	
<u>Parlung (Tibet)</u>	<u>29.24</u>	<u>96.93</u>	<u>2018-2019</u>	<u>4600-5800</u>	<u>2.19</u>	<u>679</u>	<u>This Study</u>
<u>CMBC (Canada)</u>	<u>50.32</u>	<u>-122.48</u>	<u>2006-2008</u>	<u>1375-2898</u>	<u>10.29</u>	<u>1113</u>	<u>Shea and Moore (2010)</u>
<u>AVDM (Italy)</u>	<u>46.42</u>	<u>10.62</u>	<u>2010-2011</u>	<u>2650-3769</u>	<u>7.94</u>	<u>1233^b</u>	<u>Carturan et al. (2015)</u>
<u>Tsanteleina (Italy)</u>	<u>45.48</u>	<u>7.06</u>	<u>2015</u>	<u>2800-3445</u>	<u>13.76</u>	<u>805</u>	<u>Shaw et al., (2017)</u>
<u>Arolla (Switzerland)</u>	<u>45.97</u>	<u>7.52</u>	<u>2010</u>	<u>2550-3520</u>	<u>7.28</u>	<u>1663</u>	<u>Ayala et al. (2015)</u>
<u>McCall (USA)</u>	<u>69.31</u>	<u>-143.85</u>	<u>2004-2014</u>	<u>1375-2365</u>	<u>-2.28</u>	<u>500</u>	<u>Troxler et al. (2020)</u>
<u>Juncal Norte (Chile)</u>	<u>-33.01</u>	<u>-70.09</u>	<u>2007-2008</u>	<u>2900-5910</u>	<u>6.58</u>	<u>352</u>	<u>Ayala et al. (2015)</u>
<u>Greve (Chile)</u>	<u>-48.88</u>	<u>-73.52</u>	<u>2015-2016</u>	<u>0-2400</u>	<u>-0.1</u>	<u>6450^c</u>	<u>Bravo et al. (2019a)</u>
<u>Pasterze (Austria)</u>	<u>47.09</u>	<u>12.71</u>	<u>1994</u>	<u>2150-3465</u>	<u>12.66</u>	<u>2761</u>	<u>Greuell and Böhm. (1998)</u>
<u>Universidad^d (Chile)</u>	<u>-34.69</u>	<u>-70.33</u>	<u>2009-2010</u>	<u>2463-4543</u>	<u>8.24</u>	<u>474</u>	<u>Bravo et al. (2017)</u>
<u>Peyto^d (Canada)</u>	<u>51.66</u>	<u>-116.55</u>	<u>2011</u>	<u>2260-3000</u>	<u>2.94</u>	<u>800</u>	<u>Pradhananga et al. (2020)</u>
<u>Djankuat^d (Russia)</u>	<u>43.20</u>	<u>42.77</u>	<u>2017</u>	<u>3210-4000</u>	<u>12.13</u>	<u>950</u>	<u>Rets et al. (2019)</u>

368 ^a MSAT corrected from ERA5 grid height to mean elevation of glacier using the environmental lapse rate

369 ^b Average for 1979-2009. Precipitation for 2010-2011 was above average at ~1400 mm (L. Carutran, pers
370 comm)

371 ^c Value taken from Bravo et al. (2019b)

372 ^d Glaciers where the ELR was used to distribute temperature for k1/k2 calculation. See text for details.

373

374

375 Finally, we group the derived k_2 sensitivities of the SM10 approach against the climatology that
376 describes the given glacier(s) location. For this, we consider the mean summer (JJAS or DJFM in
377 the southern hemisphere) air temperature (MSAT) and the total annual precipitation for the year(s)
378 of study at each location (Table 2). MSAT is derived from the ERA5 product for the glacier
379 centroid location and corrected to the mean glacier elevation by the *ELR*. However, total
380 precipitation from ERA5 has been shown to have considerable bias when tested against in-situ
381 observations (e.g. Betts et al., 2019), and so we provide the best available value from the relevant
382 literature (Table 2). We note that a full analysis of the local climate is beyond the scope of this
383 work, though we attempted a generalised analysis in order to link any clear differences in the
384 global datasets to climatological influences.

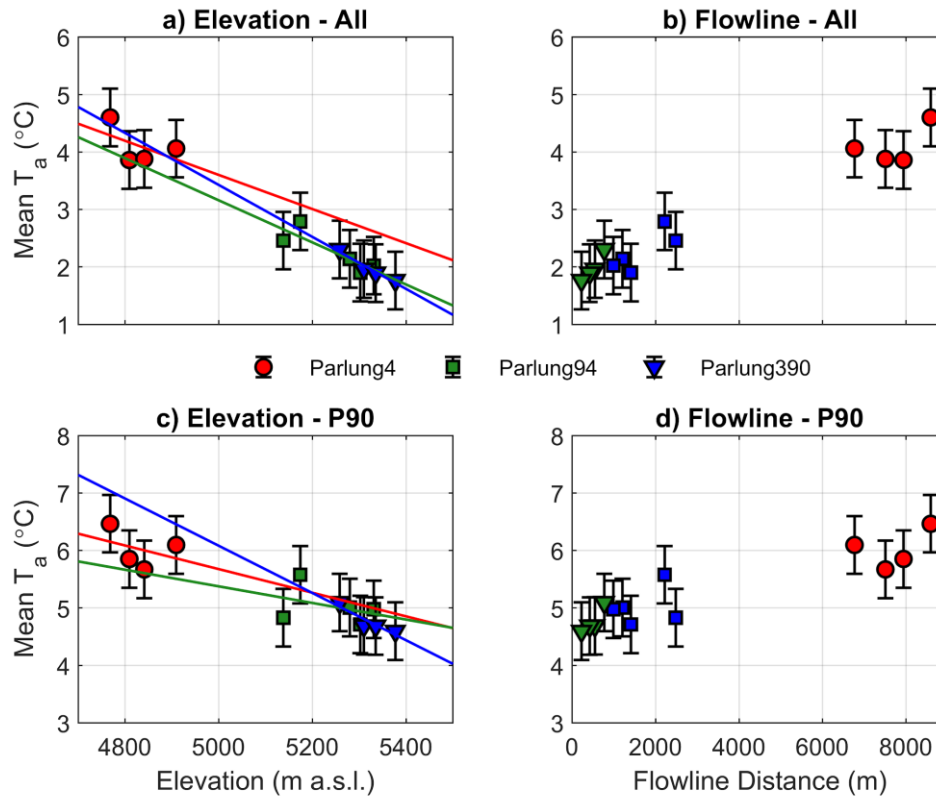
385

386 5. Results

387 5.1. Variability of on-glacier air temperatures

388 Figure 3 shows the mean T_a as a function of elevation and flowline distance for the Parlung
389 glaciers for all conditions and for the warmest 10% of AWS_Off observations (P90). The average
390 of all hours ($n = 3312$) reveals a generally linear relationship with the glacier elevation (Figure
391 3a) and flowline distance (Figure 3b), resulting in mean on-glacier lapse rate (mean R^2 with
392 elevation) equivalent to $-3.0^\circ\text{C km}^{-1}$ (0.92), $-3.7^\circ\text{C km}^{-1}$ (0.71) and $-4.5^\circ\text{C km}^{-1}$ (0.81) for
393 Parlung4, Parlung94 and Parlung390, respectively. For P90 hours ($n = 312$), mean T_a
394 demonstrates a poorer fit to elevation and with flowline distance for Parlung4 (mean R^2 with
395 elevation = 0.12, and flowline = 0.20) and Parlung 94 (mean R^2 with elevation = 0.13 and flowline
396 = 0.09). For the small Parlung390 Glacier, T_a remains strongly related to elevation ($R^2 = 0.84$)
397 and flowline ($R^2 = 0.82$) under P90 conditions. The equivalent mean on-glacier ‘lapse rates’ for
398 P90 hours are $-2.1^\circ\text{C km}^{-1}$, $-1.4^\circ\text{C km}^{-1}$ and $-4.1^\circ\text{C km}^{-1}$. Nevertheless, assuming a ~~calculated~~

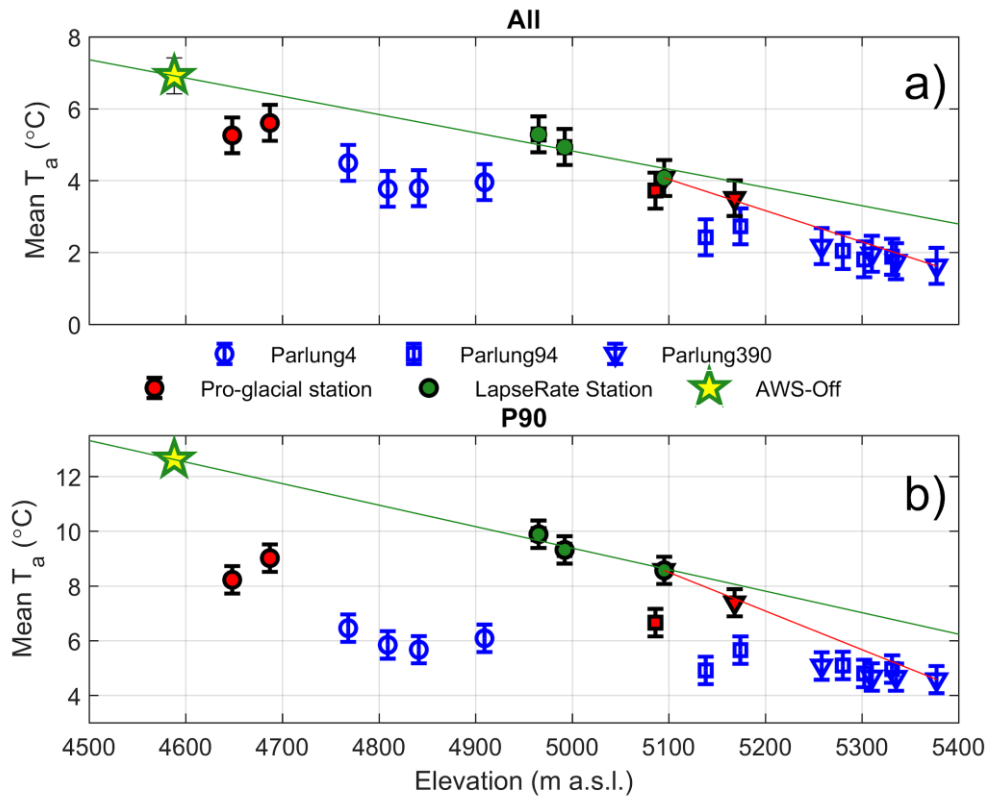
399 0.5°C uncertainty of the observations for P90 conditions (Figure 3c and d), the mean of
 400 observations still lies along a linear fit line. However, for given hours, the deviation of
 401 observations from the linear fit line exceeds 3°C at large flowline distances (> 7000 m) on
 402 Parlung4. In general, 2018 experienced cooler average temperatures at higher elevations, but in
 403 general, there are no marked differences between the two years of observation when comparing
 404 on-glacier T_a to glacier elevation or flowline (not shown).
 405



406
 407 Figure 3: The mean T_a against elevation and uncertainty (errorbar) for (a) all hours ($n = 3312$) and (c)
 408 P90 hours ($n = 312$). Panels (b) and (d) are the equivalent plots against flowline distance. Coloured lines
 409 show the linear fit against elevation ('lapse rate') to each glacier.
 410

411
 412 **5.2. Differences in on- and off-glacier air temperatures**

413 Comparing mean on- and off-glacier T_a at the same elevation reveals the expected behaviour
 414 associated with the glacier 'cooling effect' (Carturan et al., 2015) and a greater deviation from
 415 the calculated catchment lapse rate temperature for the warmest conditions (P90, Figure 4),
 416 indicating a reduced climate temperature sensitivity. The mean T_a observed at off-glacier T-
 417 Loggers supports the selection of those stations used for catchment lapse rate calculation (green
 418 dots in Figure 4) that are further from the potential effects of the glacier boundary layer (red
 419 markers in Figure 4). Following Carturan et al. (2015), we suggest a potential non-linear
 420 behaviour of lapse rates between AWS_Off and the top of the flowline for Parlung390, though
 421 we lack the off-glacier observations above the flowline origin to test this (Figure 4b). We therefore
 422 utilise a piecewise lapse rate at the point of the highest off-glacier lapse rate station (T1₃₉₀ - red
 423 line in Figure 4) to account for the discrepancy between the estimated and observed T_a at T6₃₉₀,
 424 which is assumed to be near to the flowline origin where climate temperature sensitivity is
 425 theoretically equal to 1 (i.e. that where the on-glacier observations = $T_{a,amb}$). are expected to match
 426 $T_{a,Amb}$.
 427



428

429

430

431

432

433

434

435

436

437

438

439

440

441

442

443

444

445

446

447

Figure 4: The mean T_a against elevation for all hours (a) and P90 hours (b), where blue markers are on-glacier T-Loggers, red markers are pro-glacial T-Loggers and green circles denote off-glacier T-Loggers used to construct an hourly variable 'catchment lapse rate' (green line), extrapolated from AWS Off (star). The red line indicates the piecewise lapse rate above the elevation of T1_390 to lapse T_a to the top of the flowline. A 0.5°C uncertainty is shown by the errorbar for each station (not applied to the lapse rate for neatness).

Figure 5 presents the hourly differences between T_{aAmb} and observed T_a at each site. The deviation of estimated and observed T_a theoretically begins at a critical temperature threshold, T^* (Shea and Moore, 2010) and this effect can be observed at T-logger sites on Parlung94 and Parlung4, particularly those at greater flowline distances. ~~Coloured by the hourly wind speeds recorded at AWS_On, the beginning of the temperature deviations (T^*) aligns glacier T_a and T_{aAmb} align well with~~until the onset of katabatic winds (on Parlung4 (and only assumed for the other glaciers due to lack of on-glacier wind observations – Figure 5). Despite being pro-glacial stations, T1₄ and T2₄ reveal a similar, albeit weaker effect of the glacier boundary layer, possibly due to larger glacier flowline and ~~sustained-effect~~extension of the katabatic wind into the pro-glacial area.

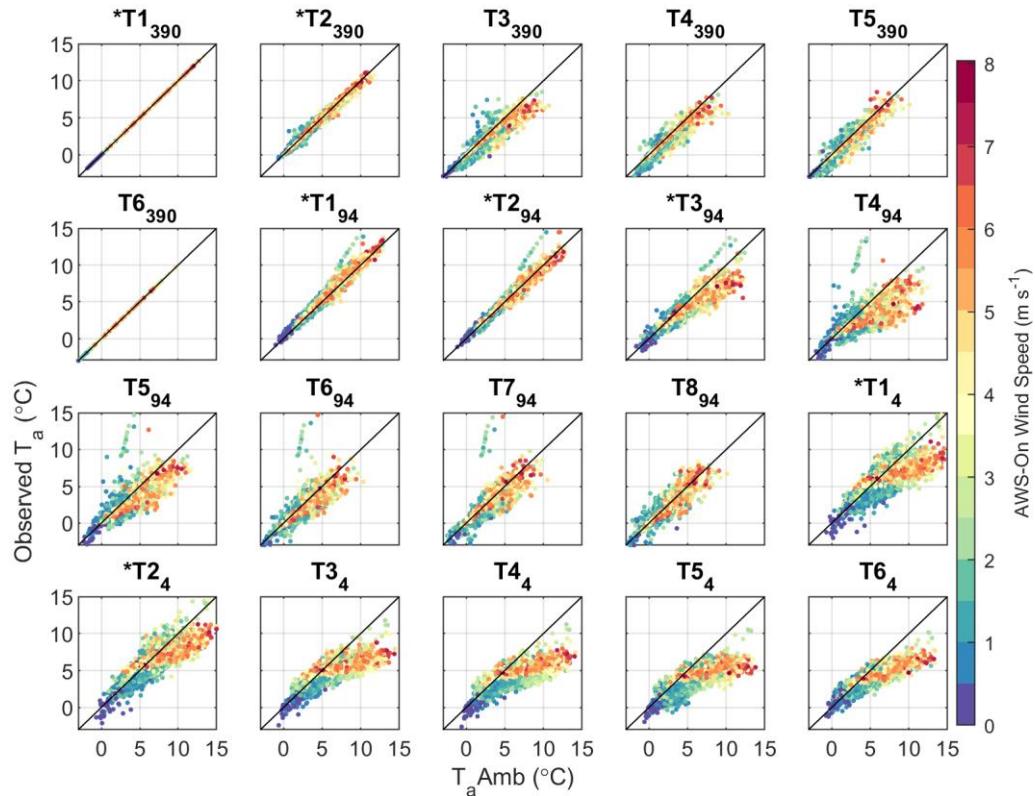
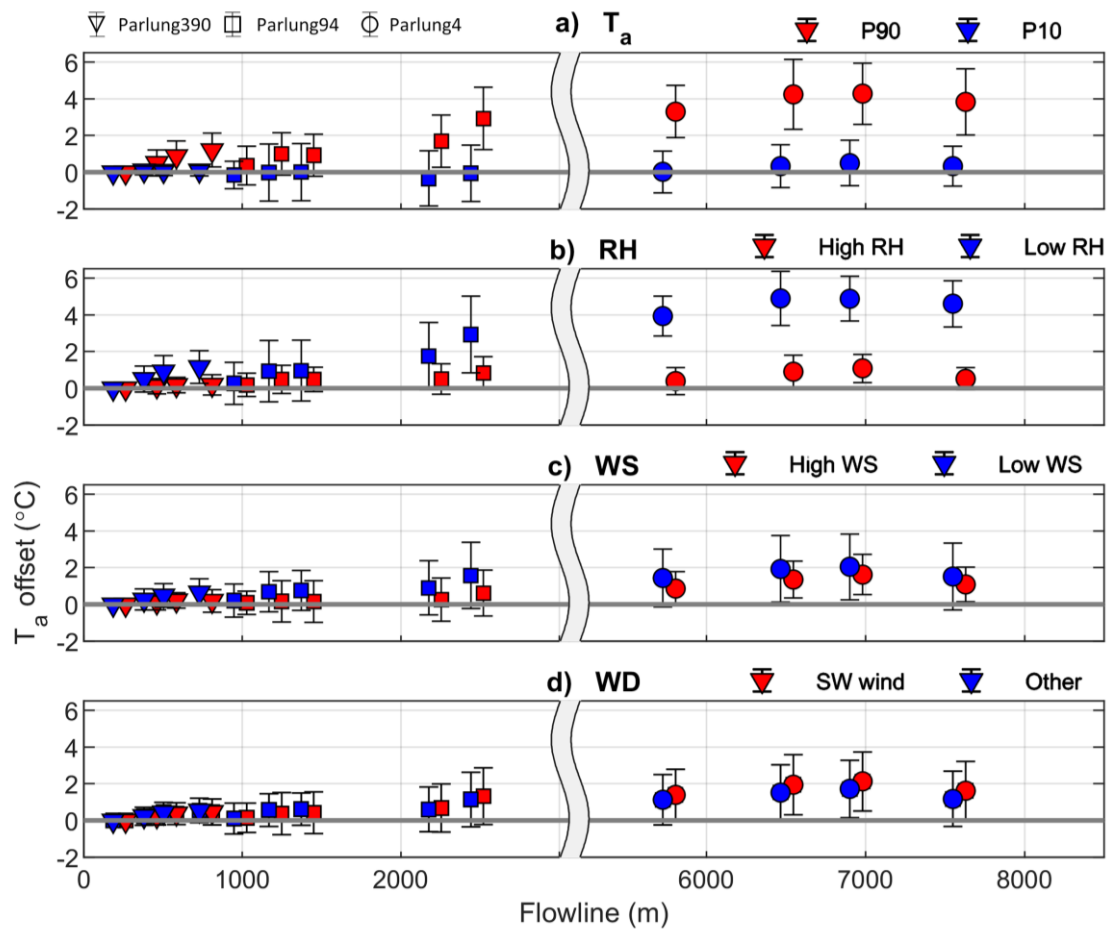


Figure 5: Estimated (T_{aAmb}) vs Observed T_a at each T-Logger location (including off-glacier T-Loggers). Individual, hourly values are coloured by the observed wind speeds at AWS On (Parlung4). * denotes stations that are off-glacier.

The mean bias offset difference of along-flowline T_a and T_{aAmb} using the catchment lapse rate is shown in Figure 6. For the coolest 10% of hours at AWS_Off (P10), there is generally minimal offset difference between T_{aAmb} and observed T_a for the entire dataset. ~~This clearly does not hold true for~~ For P90 conditions (Figure 6a), ~~as already established (Figure 4), and offsets of T_a (differences between T_{aAmb} and observed T_a) on-glacier temperatures~~ are up to 5.8°C at flowline distances ~~of \rightarrow greater than 7000 m on Parlung4~~. These effects differences appear to heighten increase beyond 2000 m along the flowline (Parlung94), though slight offsets significant differences can be witnessed for all glaciers: (different symbols in Figure 6). This is generally associated with drier conditions, and for hours of greater relative humidity (AWS_Off), offsets when conditions are small generally cooler, differences are unsurprisingly smaller (Figure 6b). Considering ‘free-air’ wind variability provided by ERA5 reanalysis, T_a offsets differences are largest for the dominant south-westerly wind direction (85% of hours) and when free-air wind speeds are smallest (Figure 6c and 6d). However, un-corrected, gridded wind speeds do not appropriately represent the local ‘free-air’ boundary conditions and thus the interaction of off-glacier wind speeds and the glacier boundary layer development remain unclear for these glaciers. For all but the coolest ambient temperatures (Figure 6a), observations at the greatest flowline distances deviate the most from the estimated values. Besides the analyses against individual meteorological variables, the differences are largest for warm/anticyclonic conditions, and lowest for cool/cyclonic conditions.



474

475 *Figure 6: The mean and standard deviation (error-bars) of hourly T_a differences ($T_{a,Amb}$ - observed)*
 476 *along the glacier flowline. Each panel depicts hourly grouping by (a) off-glacier T_a at AWS Off (P90 \geq*
 477 *10.5°C and P10 is $< 3.5^\circ\text{C}$), (b) off-glacier RH at AWS Off (high is $> 90\%$ and low is $< 70\%$), (c) wind*
 478 *speed from ERA5 (high is $> 2.5 \text{ m s}^{-1}$ and low is $< 0.7 \text{ m s}^{-1}$) and (d) dominant wind direction from ERA5*
 479 *(Southwest wind direction is considered as $180\text{-}270^\circ$). Marker shapes show the different glaciers, as in*
 480 *Figure 3 and 4. This offset is X axes are split to improve visibility at low flowline distances.*

481

482

483 The differences between $T_{a,Amb}$ and on-glacier T_a are highly variable in time, however, and
 484 related to the prevailing conditions of a given year (Figure 7). Considering the maximum daily T_a
 485 offsets differences at the on-glacier T-Logger closest to the terminus of each glacier (Table 1,
 486 Figure 2), we find that Parlung94 and Parlung4 T-loggers have similar magnitudes of T_a offsets
 487 during the mid-summer months, particularly for 2018 (Figure 7). These maximum
 488 offsets differences are in clear relation to the incoming shortwave radiation recorded recorded at
 489 AWS_Off (correlations of 0.44, 0.60 and 0.80 for Parlung390, Parlung94 and Parlung4,
 490 respectively), which are indicative of warmer ambient conditions (i.e. P90). For Parlung390 this
 491 offset is much smaller, though it varies considerably throughout the summer. For 2019, maximum
 492 daily T_a offsets on Parlung390 steadily increase during July and August then fall close to zero in
 493 September. The bias offsets maximum differences for Parlung4 and Parlung94, however, remain
 494 sizeable (Figure 7-), perhaps due to the persistence of katabatic winds over a larger flowline
 495 distance even under the relatively cooler conditions of September. Because our study period
 496 focuses on the core monsoon period (Yang et al., 2011), we do not observe the influence of
 497 monsoon arrival or cessation on the T_a variability of the Parlung Glaciers.

498

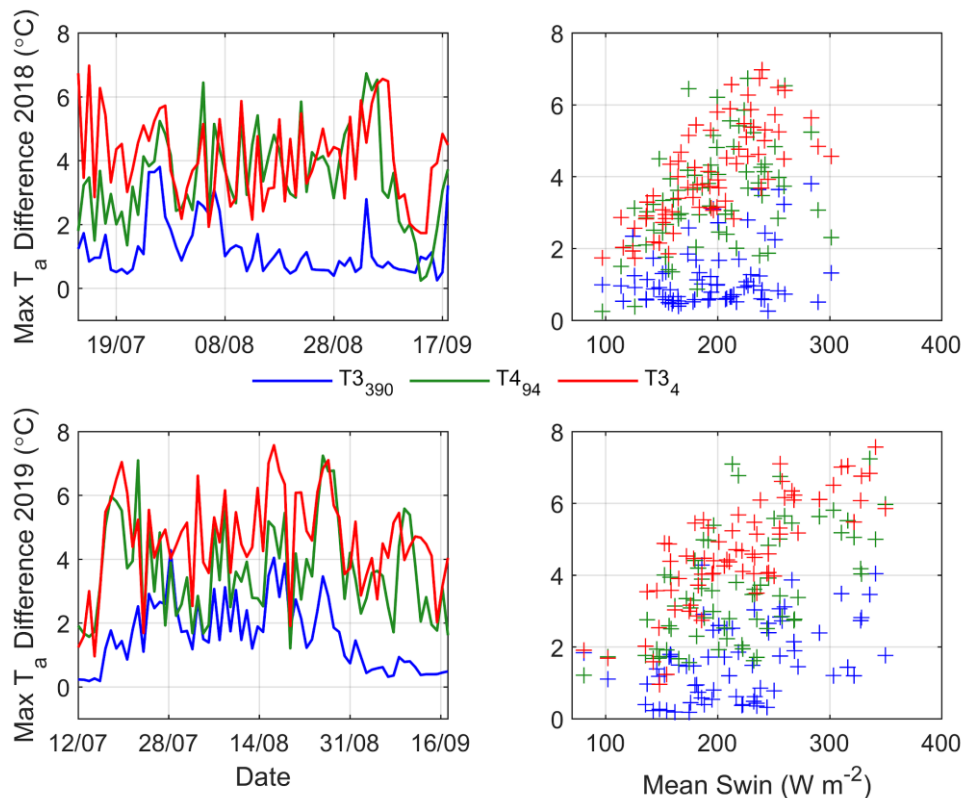
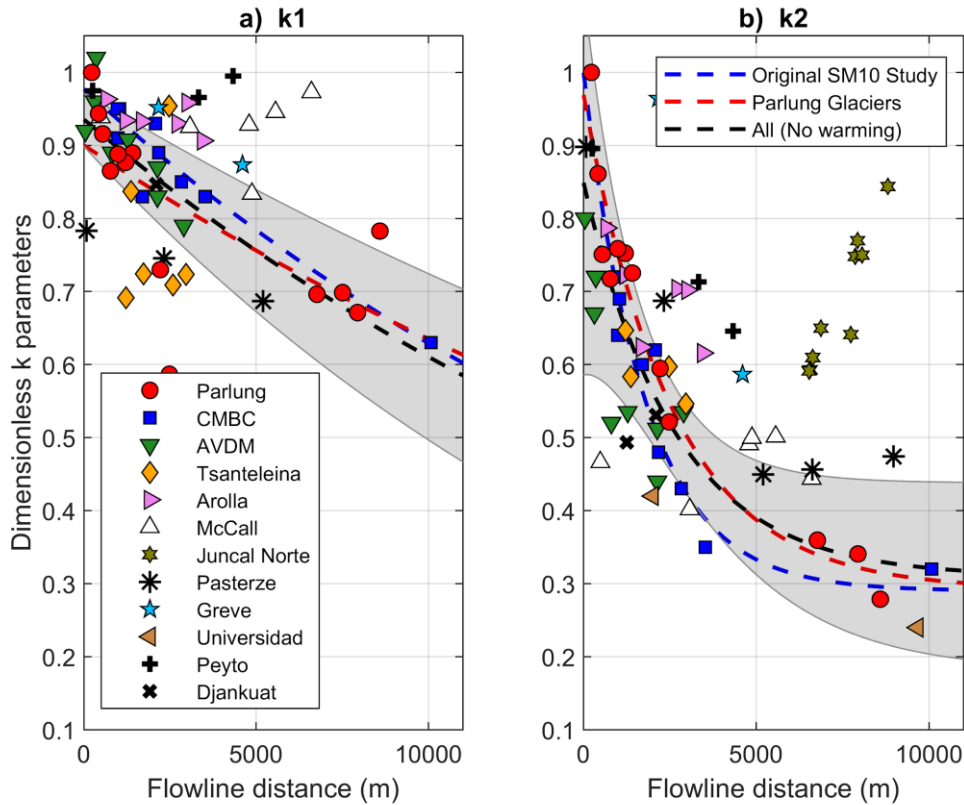


Figure 7: Maximum daily T_a differences ($T_{a,Amb}$ - observed) at the T-Logger closest to the terminus on each glacier for 2018 (top panels) and 2019 (bottom panels). Maximum daily T_a differences are plotted against mean daily incoming shortwave radiation at AWS. Off in the right hand panels.

5.3. Parameterisation of along-flowline air temperatures

Figure 8 presents the temperature sensitivities of the SM10 parameterisations approach for the Parlung glaciers in comparison to those derived for the and available distributed T_a datasets around the world (Table 2). Comparing the $k1$ and $k2$ parameters from Tibet to the original-parameters of Shea and Moore (2010), from western Canada, a similar behaviour is observable for both sites up to ~2000-3000 m of flowline distance (red and blue dashed lines), though there exists a larger variability in the calculated parameters at longer flowline distances on Parlung4 (Figure 8). Accordingly, the symbols). The exponential functions that are fitted to the observations at Parlung glaciers and the original study are notably distinct (red and blue lines in Figure 8, Table 3). This behaviour is further highlighted when observing, although within the confidence intervals of each other published or revised datasets for the context of this work (Figure 8b). A 'global' parameterisation. Fitting an exponential function for all sites where a down-glacier decrease in elmatietemperature sensitivity ($k2$) is evident (black dashed linesline in Figure 88b) clearly misrepresents many of the observations, particularly those at greater flowline distances, balancing the behaviours reported for different sites.



521

522 *Figure 8: The calculated k_1 and k_2 sensitivities as a function of the flowline distance of each observation*
 523 *on the Parlung glaciers (red circles) and other, global datasets (Table 2). The dashed blue and red lines*
 524 *show the fitted exponential parameterisation of Shea and Moore (2010) and this study, respectively. The*
 525 *dashed black line and shaded area denotes the equivalent parameterisation for all observations without a*
 526 *large increase in sensitivity on the glacier terminus ('warming effect' - explicitly excluding data from*
 527 *McCall, Juncal Norte and Djankuat). The shaded area represents the 95% confidence interval of this fit*
 528 *line.*

529

530

531 *Table 3: The coefficients of the original SM10 model and those fitted to the k_1 and k_2 sensitivities on the*
 532 *Parlung glaciers and all glaciers where no warming effect was evident (see Figure 10).*

<u>Model</u>	<u>$k_1 = \beta_1 * \exp(\beta_2 * DF)$</u>	<u>$k_2 = \beta_3 + \beta_4 * \exp(-\beta_5 * DF)$</u>
<u>CMBC (Shea and Moore, 2010)</u>	<u>$\beta_1 = 0.977$</u> <u>$\beta_2 = -4.4e-5$</u>	<u>$\beta_3 = 0.29$</u> <u>$\beta_4 = 0.71$</u> <u>$\beta_5 = 5.6e-3$</u>
<u>Parlung</u>	<u>$\beta_1 = 0.894$ (0.805,0.983)</u> <u>$\beta_2 = -2.972e-5$ (-5.543e-5,-4.0e-6)</u>	<u>$\beta_3 = 0.349$ (0.241,0.456)</u> <u>$\beta_4 = 0.624$ (0.492,0.757)</u> <u>$\beta_5 = 4.4e-3$ (1.7e-4,7.2e-4)</u>
<u>All (no increased sensitivity on glacier terminus)</u>	<u>$\beta_1 = 0.923$ (0.886,0.96)</u> <u>$\beta_2 = -3.375e-5$ (-5.543e-5,-4.0e-6)</u>	<u>$\beta_3 = 0.343$ (0.225,0.46)</u> <u>$\beta_4 = 0.511$ (0.38,0.642)</u> <u>$\beta_5 = 4.2e-3$ (1.5e-4,6.9e-4)</u>

533

534

535

536

537

538

539

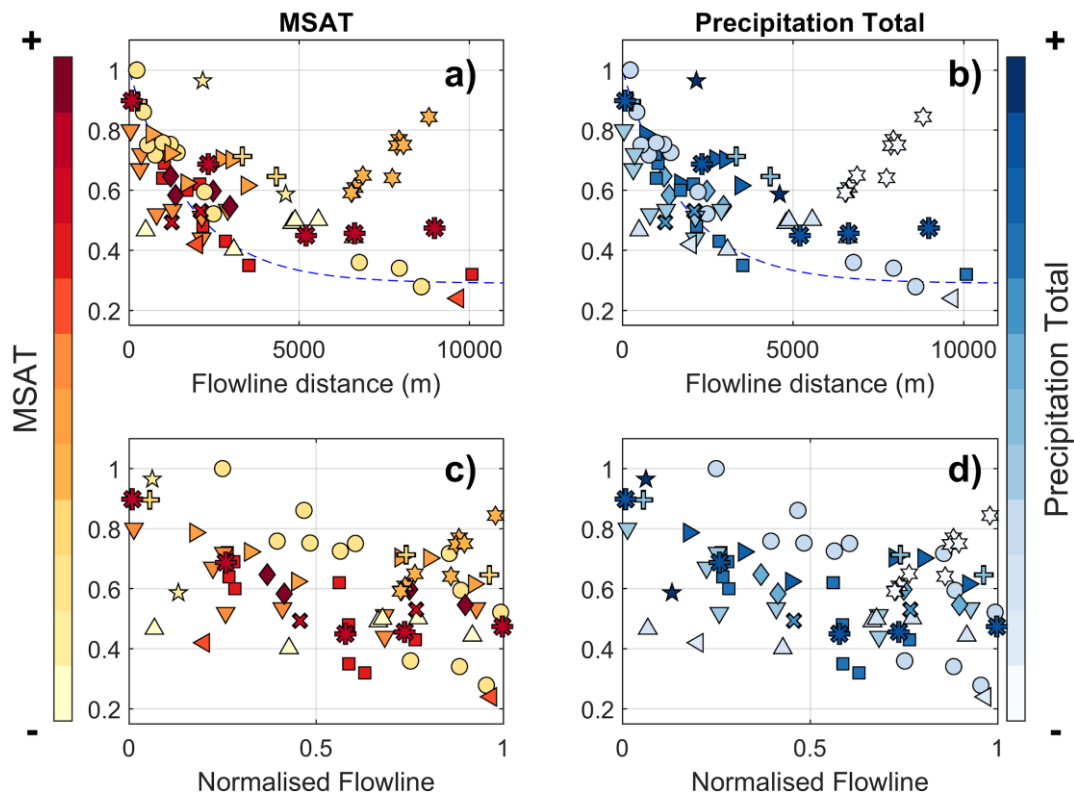
Notably, observations at McCall Glacier, Alaska relate very well to ambient T_a under cooler conditions, with **almost** k_1 values remaining > 0.9 . Above the T^* threshold, however, the relationship of observed and estimated T_a results in increasing k_2 along the flowline, in contradiction to the majority of the other datasets. Nevertheless, this data also confirms the increased **climatic temperature** sensitivity on the glacier terminus (Troxler et al., 2020) as evident

540 with datasets for Tsanteleina (Shaw et al., 2017), Arolla and Juncal Norte (Ayala et al., 2015).
 541 Observations at Parlung4 and Universidad Glacier (Bravo et al., 2017) emphasise the strong
 542 decrease in climate temperature sensitivity at large flowline distances (~10,000 m) previously
 543 only witnessed from one location on Bridge Glacier, Canada (Shea and Moore, 2010). At these
 544 stations, changes in on-glacier T_a are less than a third of the equivalent change in T_{aAmb} .

545
 546 Figure 9 shows the k_2 parameters plotted against flowline distance, coloured by rankings of
 547 MSAT and precipitation totals (Table 2). The warmest of the investigation investigated sites
 548 (during the measurement years) appear to lie closer along to the original SM10 parameterisation
 549 until exponential function up to ~4000 m, whereas deviation of the k_2 parameters from this line
 550 appears larger for observations at the relatively cold sites (Greve, McCall and Arolla Peyto –
 551 Figure 9a). The main exception to this is for Juncal Norte (Petersen and Pellicciotti, 2011; Ayala
 552 et al., 2015), which demonstrates a high and rapidly increasing sensitivity of ambient T_a at the
 553 greatest flowline distances.

554 No clear patterns are visible within relation to mean annual precipitation totals, although, though
 555 the observations distinct behaviour at Juncal Norte are noted as Glacier corresponds to the driest
 556 of the study sites considered (Figure 9b).

557



558

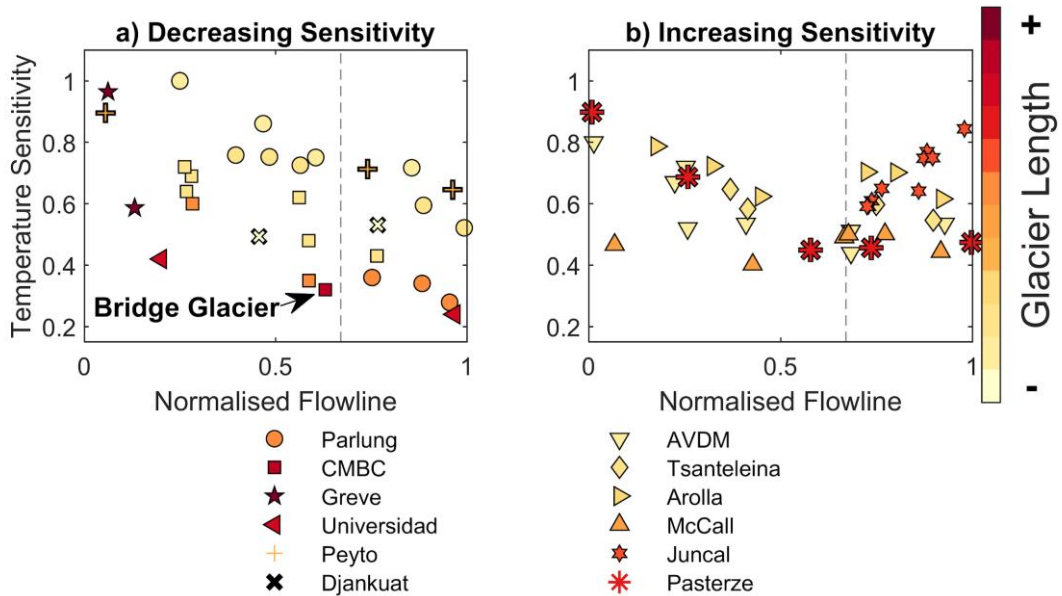
559 Figure 9: The k_2 sensitivities as a function of flowline distance (top) and a normalized distance, considering
 560 the total flowline distance for the year of study (bottom). The individual glaciers of grouped studies
 561 (Parlung, CMBC and AVDM) are separated and normalized by the individual glacier length (symbols as
 562 in Figure 8). Glaciers are coloured by rankings of the mean summer air temperatures (MSAT - left) and
 563 precipitation total (right). The original SM10 parameterisation is retained in the top panels.

564

565

566 A clear difference between the station observations of CMBC Shea and Moore (2010) and Parlung
 567 glaciers at large flowline distances (Figure 8) is the total distance of that station observation
 568 from the glacier terminus, which suggests a possible difference in processes being compared occurring
 569 between sites. Accordingly, we plot the k_2 parameters as a function of the normalized flowline;
 570 (Fig 9c and d), adjusted by the total length of glacier under for the year(s) of observation (Table

571 2). A slight trend toward lower k_2 values (lower sensitivity to ambient T_a) is observable for
 572 relatively warmer regions, though no clear pattern emerges for MSAT (Figure 9c) or precipitation
 573 totals (Figure 9d). The largest flowline distance observation of the entire dataset (Figure 9a) in
 574 fact extends only ~60% of the total glacier length (Bridge Glacier - CMBC), neither representing
 575 the smallest ~~climate~~ temperature sensitivity (Figure 8b), nor ~~the an~~ increasing ~~climate~~ temperature
 576 sensitivity witnessed at the terminus of the glacier (and estimated using the ModGB model) by
 577 other studies (Ayala et al., 2015). In fact, by subjectively grouping glacier sites; Troxler et al.,
 578 2020). We group glaciers by the presence of the relative down-glacier cooling (decreasing
 579 sensitivity) and warming (decreasing followed by (or absence) of an increasing temperature
 580 sensitivity) along on the terminus in Figure 10. We find that there is no clear relation between the
 581 total length of the glacier length, one can observe that this effect is absent and increasing
 582 temperature sensitivity, which is seen for the both smaller and larger glaciers (Figure 10a), albeit
 583 limited by lack of observations across an entire glacier in most cases. 10b). For those glaciers
 584 where the pattern of down-glacier a temperature sensitivity increase (a relative 'ModGB'
 585 warming effect - Figure 1a) is evident, it is found only beyond ~70% on the lowest 30% of
 586 the total glacier flowline distance terminus (Figure 10b – vertical dashed line). Up to this distance,
 587 no increase in
 588



589 Figure 10: The k_2 sensitivity is seen from the data along the normalized flowline compared to total glacier
 590 length (colour bar). Glaciers have been grouped in two clusters: a) those with down-glacier decreasing
 591 sensitivity, and b) those with increasing sensitivity towards the glacier terminus.
 592

593
 594

595 6. Discussion

596 6.1. Relevance of the findings from Parlung Glaciers
 597 The Our observations of along-flowline T_a on the glaciers in the Parlung catchment add yet provide
 598 more evidence of the spatial variability of the glacier cooling and dampening effect (Oerlemans,
 599 2001; Carturan et al., 2015; Shaw et al., 2017) and highlights the need to appropriately estimate
 600 its behaviour for use in glacier energy balance and enhanced temperature index melt models
 601 (Petersen and Pellicciotti, 2011; Shaw et al., 2017; Bravo et al., 2019, 2019a). It has long since
 602 been observed that a static lapse rate is inappropriate for characterising the spatio-temporal
 603 variability of T_a , both within the KBL (Greuell et al., 1997; Konya et al., 2007; Marshall et al.,
 604 2007; Gardner et al., 2009; Petersen and Pellicciotti, 2011) and outside the glacier boundary layer
 605 in adjacent valleys (Minder et al., 2010; Immerzeel et al., 2014; Gabbi et al., 2014; Heynen et al.,

2016; Jobst et al., 2016). Despite this, the lack of locally available observations often requires modellers to force ~~model simulations~~ models with the nearest off-glacier record of T_a and extrapolate it based upon the *ELR* value as a default. In the case of Tibetan glaciers, model studies have often derived static lapse rates between on-and off-glacier stations (Huintjes et al., 2015) or ~~used static values to extrapolate or~~ downscale T_a with a correction factor based upon a single on-glacier location (e.g. Caidong and Sorteberg, 2010; Yang et al., 2013; Zhao et al., 2014). To the ~~author's~~ authors' knowledge, this is the first time that such detailed information regarding spatio-temporal variations in T_a have been presented for a glacier of the Tibetan Plateau. Because glaciers of the south-eastern Tibetan Plateau have been shown to be particularly susceptible to increases in T_a (Wang et al., 2019), accurately parameterising T_a along glaciers of differing size is highly relevant for present and future melt modelling attempts. This is especially true where glaciers begin to shrink or fragment (Munro and Marosz-Wantuch, 2009; Jiskoot and Mueller, 2012; Carturan et al., 2015) and become more sensitive to ambient air temperatures due to a lack of katabatic boundary layer development (Figures 6 and 7).

The summer monsoon exerts a strong control on the energy and mass balance of Tibetan glaciers (Yang et al., 2011; Mölg et al., 2012; Zhu et al., 2015). Although our dataset spanned two summers of only the core monsoon period for this region (Yang et al., 2011), we have shown that the sensitivity of the glacier to external temperature changes (shown by ~~T_a bias offset~~ on-glacier and ambient T_a differences) has a sizeable temporal variability that can be controlled by the monsoon weather conditions (such as ambient air temperature, humidity and incoming radiation) and can sometimes be independent of the glacier size (Figure 7). Whilst we cannot determine the impact of monsoon timing and intensity upon the ~~climate~~ temperature sensitivity of these glaciers with the current dataset, we are able to determine that the observed relationship to flowline distance is consistent to that of other regions of the world (Figure 8). Future work on Tibetan glaciers should attempt to extend monitoring to the pre-monsoon period to identify if a seasonal onset for the changing glacier ~~climate~~ temperature sensitivity can be defined, and how the monsoon may affect it. Particular focus should be given to understand the local meteorological conditions for each glacier, as this may explain some of the variability in T_a offset values, and why they may sometimes be independent of the along-flowline distance (Figure 7).

6.2. Parameterising glacier ~~climate~~ temperature sensitivity

In this study, we discuss the ~~climate~~ temperature sensitivity of on-glacier T_a based upon observations above a threshold ambient temperature for the onset of katabatic conditions (T^*). This sensitivity to ambient temperature during relatively warm conditions, indicated by the k_2 parameter of Shea and Moore (2010) (Figure 1), demonstrates a generally consistent behaviour between the T-logger observations of Parlung glaciers and those where this model had been previously implemented (Shea and Moore, 2010; Carturan et al., 2015). ~~It also resulted in a similar parameterisation, albeit with a slightly greater sensitivity to the ambient temperature (i.e. larger k_2 values – Figure 8b). Whilst the newly presented dataset for~~ While data from the Parlung catchment provides an important confirmation of the ~~climate~~ temperature sensitivity for some Tibetan glaciers, further studies of individual glaciers can provide only local parameterisations for ~~climate~~ temperature sensitivity that may not be applicable to other sites. Accordingly, we have made here ~~a one of the first attempt~~ attempts at combining many of the published datasets regarding distributed T_a on mountain glaciers around the world (Table 2) to examine the potential ~~for~~ generalisability transferability of a model accounting for ~~climate~~ temperature sensitivity (Figure 8).

We found a sizeable spread in the ~~climate~~ temperature sensitivities of T_a for the on-glacier datasets considered, though a consistently rapid decrease of sensitivity along glacier flowlines is found for most sites up until ~2000-3000 m of distance (Figure 8b). While localised meteorological and topographic factors likely interact to explain the spread of sensitivities at small flowline distances (Figure 8b), the results suggest that small glaciers with flow lengths < 1000 m would reflect a 0.7-0.8 sensitivity to changes in T_{aAmb} . Beyond this distance, the ~~climate~~ temperature sensitivities notably follow one of two patterns; a continued, albeit less rapid decrease in

661 sensitivity (~~more~~ generally following the model proposed by Shea and Moore (2010)), or a
662 tendency toward increasing sensitivity at the largest flowline distances (~~more related to those~~
663 ~~findings of in agreement with~~ the ‘ModGB’ model - Figure 1a). With reference to the relative T_a
664 differences among only on-glacier observations, these have been termed as down-glacier
665 ‘cooling’ or ‘warming’, respectively for many past studies (Ayala et al., 2015; Carturan et al.,
666 2015; Shaw et al., 2017; Troxler et al., 2020). Whilst the former is generally associated with
667 relatively warmer regions of study (Figure 9), such as the ~~Canadian Rockies~~ southern Coast
668 Mountains (Shea and Moore, 2010) or Universidad Glacier (Bravo et al., 2017), no strong
669 relationship of the climate setting exists between these sites to explain the magnitude of the
670 ~~climate~~ temperature sensitivity (i.e. the strength of the glacier cooling and dampening effect) nor
671 the observed increases in ~~climate~~ temperature sensitivity on glacier termini (Ayala et al., 2015;
672 Shaw et al., 2017; Troxler et al., 2020).

673
674 Interestingly, we noted that the ~~most distant~~ station observation with the largest flowline distance
675 used to derive the parameterisation by Shea and Moore (2010) was located only around 60% of
676 the total glacier flowline distance (Bridge Glacier - Figure 10), whereas data presented by other
677 studies, provided observations up to the glacier terminus (Greuell and Böhm, 1998; Ayala et al.,
678 2015; Shaw et al., 2017; Troxler et al., 2020), therefore potentially parameterising different effects
679 of the glacier boundary layer. It has been suggested that observations at large flowline distances
680 (such as that on Parlung4 or Bridge Glacier) represent a segment of the boundary layer where the
681 near-surface layer becomes highly insensitive to the ambient free-air temperature fluctuations
682 (point ‘3’ in Figure 1a and d). This phenomenon has been shown to be sustained over large fetch
683 distances by an increasing depth of the glacier wind layer (van den Broeke et al., 1997; Greuell
684 and Böhm, 1998; Shea and Moore, 2010, Jiskoot and Mueller, 2012). However, as air parcels
685 travel down-glacier toward the glacier terminus (point ‘4’ in Figure 1a and d), they potentially
686 encounter warm air entrainment due to a divergent boundary layer (Munro, 2006), up-valley
687 winds (Pellicciotti et al., 2008; Oerlemans, 2010; Petersen and Pellicciotti, 2011), large changes
688 in surface slope and the dominance of adiabatic heating over sensible heat losses (Greuell and
689 Böhm, 1998) or heating from debris-covered ice at the terminus (Brock et al., 2010; Shaw et al.,
690 2016; Steiner and Pellicciotti, 2016; Bonekamp et al., 2020). These are effects of the glacier
691 boundary layer that the ModGB model was designed to account for, though we did not explicitly
692 test this within our study due to a requirement for more data and a greater number of parameters
693 and assumptions (Shaw et al., 2017). The strength of this so called along-glacier ‘warming effect’
694 could therefore be governed by local topography (adjusting the boundary layer convergence or
695 divergence) or the total glacier flowline distance and the large fetch of a cool air parcel
696 overcoming the competing effect of warm, up-valley winds (Figure 1d - as seen at T_{24} in Figure
697 5).

698
699 By ~~subjectively~~ grouping glaciers by the presence of the observed increase in ~~climate~~ temperature
700 sensitivity and normalising the flowline distance of the observations by the total flowline for each
701 glacier, we identify that the relative increases in ~~climate~~ temperature sensitivity begin at ~ 70%
702 of the total flowline distance (Figure 10). A smaller ~~climate~~ temperature sensitivity can be
703 observed for larger glaciers (Figure 10a), which is consistent with the development of the *KBL*
704 over a large fetch (Greuell and Böhm, 1998; Shea and Moore, 2010), though the length itself
705 indicates nothing clear about why greater ~~climate~~ temperature sensitivity exists for some glacier
706 termini (Figure 10b).

707
708 The clear outlier of these datasets is Juncal Norte Glacier in Chile (Figure 8b). It is interesting to
709 note that Juncal Norte is the only reported case in the literature on T_a variability where the warmest
710 hours of the afternoon correspond to the dominance of an up-valley, off-glacier wind (Pellicciotti
711 et al., 2008; Petersen and Pellicciotti, 2011). Counter to the typical role of the dominant, down-
712 glacier wind layer for these warmest afternoon hours (Greuell et al., 1997; Greuell and Böhm,
713 1998; Strasser et al., 2004; Jiskoot and Mueller, 2012; Shaw et al., 2017; Troxler et al., 2020), up-
714 valley winds on Juncal Norte seemingly erode the along-flowline reduction in
715 ~~climate~~ temperature sensitivity (along-flowline cooling) up to a distance along the flowline where

716 it is theoretically at its maximum (point '3' in Figure 1). Evidence from other glaciers suggest
717 that this point is close to upper observations for Juncal Norte at ~70% of the total flowline (Figure
718 10b), though further observations on Juncal Norte Glacier would be required to test this.

719
720 Finally, the extent to which a glacier terminus is constrained by high valley slopes may be an
721 additional explanatory factor for the occurrence of increasing temperature sensitivities on some
722 glaciers (Figure 10). While this may limit the suggested boundary layer divergence (Munro,
723 2006), it may equally promote greater warming due longwave emission from valley slopes (e.g.
724 Strasser et al., 2004; Ayala et al., 2015). We calculated the terminus width/ length ratio of each
725 glacier and compared it to the presence of increasing temperature sensitivity on the terminus
726 (supplementary Figure S4), revealing a potential relationship between the two. However, given
727 the available data for this study and the unknown extent to which longwave emission may affect
728 a fast moving air parcel (Ayala et al., 2015), a dedicated study would be required to further address
729 this hypothesis.

730 6.3. *Future directions for researching air temperatures on glaciers*

731 A limitation of our work is the dependency of the derived 'global' ~~climatic~~ temperature
732 sensitivities (Figure 8b) to the available off-glacier data and the published lapse rates to
733 extrapolate them to the relevant elevations on-glacier. In our case, we are able to identify a
734 potentially non-linear lapse rate of T_a for the highest elevations over Parlung94 and
735 Parlung390 (Figure 4). Although we cannot confirm this without off-glacier observations above
736 the top of the flowline (Carturan et al., 2015), we are able to well constrain ambient air
737 temperature distribution using hourly observations at several off-glacier locations to derive the
738 best possible 'catchment lapse rate'. For other datasets (Table 2), we rely upon the available off-
739 glacier data and lapse rates that are not derived in a consistent manner. The derivation of flowline
740 distances from the DEM are also not consistent between the prior studies (Shea and Moore, 2010;
741 Carturan et al., 2015; Shaw et al., 2017; Bravo et al., ~~2019~~2019a; Troxler et al., 2020), and may
742 hold some small influence on the derived parameterisations (Table 3), particularly at lateral
743 locations on the glacier (not explored here), that can be subject to different micro-meteorological
744 effects (van de Wal, 1992; Hannah et al., 2000; Shaw et al., 2017). Equally, the uncertainty of the
745 actual observations (e.g. section 3.2) is hard to clearly define due the variable instrumentation
746 (sensors and radiation shielding), on-glacier location and local topographic and micro-
747 meteorological effects of each study site (Table 2). Because our study, and many similar studies
748 of this kind, did not have artificially ventilated radiation shields available, the uncertainty of the
749 measured T_a is difficult to quantify. We consider this to be less problematic at large flowline
750 distances, where good ventilation to the sensors is often provided by the glacier katabatic wind
751 layer even under warm conditions. However, at short flowline distances in the glacier
752 accumulation zones, uncertainty of both the on-glacier observations and ambient T_a extrapolation
753 is larger. Artificially ventilated radiation shields are not commonplace in glaciological research
754 due to the additional power demands that often cannot be met, though would be strongly
755 encouraged for further research into the temperature sensitivity of mountain glaciers. Further
756 work on a unified model of estimating T_a should need to address these issues, perhaps with further,
757 dedicated analyses.

758
759 In our study, we apply the parameterisation of Carturan et al. (2015) to derive along-flowline
760 values of the theoretical onset of the KBL (T^*). While these values appear appropriate for our case
761 studies (based upon manual inspection), they were derived for a ~~more limited numbers~~ smaller
762 sample size of total observations. We experimented with a static T^* value of 5°C in order to test
763 the sensitivity of our analysis to the assumptions of T^* , though ~~found a minimal change in our~~
764 ~~derived k_2 sensitivities (not shown).~~ we found negligible sensitivity of derived k_2 on T^* (not
765 shown). Similarly, a sensitivity to the choice of constant lapse rate for those sites without available
766 lapse rate information (Table 2) proved to have only a small influence on the derived k_1 and k_2
767 values.

770 Finally, in this study we assess climatic temperature sensitivity based upon ambient air
771 temperatures above ~~this~~ the T^* threshold. ~~We identify, however, that this~~ This is partly different
772 to the ‘climatic sensitivity’ presented by earlier works (Greuell et al., 1997; Greuell and
773 Böhm, 1998; Oerlemans, 2001; 2010), which considered ~~all hours of the on-glacier observations~~
774 ~~when comparing to extrapolated off-glacier T_a . In some instances, over estimation of on-glacier~~
775 ~~T_a also for cooler conditions may produce a consistent an~~ ‘all-hour’ climatic temperature
776 sensitivity value (i.e. ~~where k_1 and k_2 not thresholding~~ sensitivities ~~are similar by katabatic wind~~
777 onset - Figure 1b). However, ignoring ~~separate effects (k_1 and k_2) due the rise~~ the differences in
778 temperature sensitivity before and after the onset of the KBL (Figure 1c, Figure 5) is arguably an
779 over-simplification and therefore does not aptly enable
780 one to correctly describe the two observed behaviours ~~separated by an onset event~~ (Shea and
781 Moore, 2010; Jiskoot and Mueller, 2012). Accordingly, we caution somewhat the direct
782 comparison of the climatic temperature sensitivity presented here and ~~that~~ the ‘climatic sensitivity’
783 of previous works, ~~though~~.

784 We consider the SM10 approach and the use of k_2 to be an appropriate indicator of
785 climatic temperature sensitivity for ~~this mountain glaciers in future work going forward. As~~
786 ~~previously mentioned, we have considered the approach of Shea and Moore (2010) to be a more~~
787 generalizable this type. This approach is an easily adaptable method for calculating glacier
788 climatic temperature sensitivity and thus estimating on-glacier T_a . However, the competing effects
789 of glacier katabatic and up-valley winds/debris or valley warming need to be incorporated to
790 address the challenges that less simplistic methods (i.e. ModGB) were designed for.

791
792 Based upon the findings of this work, we recommend that future research i) attempt to standardise,
793 where possible, the measurement and comparison of off- and on-glacier air temperature,
794 potentially exploring more the use of artificially-ventilated radiation shields that are less prone to
795 heating errors (Georges and Kaser, 2002; Carturan et al., 2015), ii) instrument glaciers of varying
796 size in the same catchment to explore the relative importance of glacier size and local
797 meteorological conditions (Figure 7), and iii) model the detailed interactions of air flows on ~~the~~
798 glacier termini using, for example, large eddy simulations (Sauter and Galos, 2016; Bonekamp et
799 al., 2020) in order to identify possible drivers of the observed increase in climatic temperature
800 sensitivity for certain glaciers glacier areas (point ‘4’ in Figure 1).

802 7. Conclusions

803 We presented a new dataset of distributed on-glacier air temperatures for three glaciers of
804 different size in the south-east Tibetan Plateau during two summers (July - September). We
805 analysed the along-flowline air temperature distribution for all three glaciers and compared them
806 to the estimated ambient temperatures derived from several, local off-glacier stations. Using this
807 information, we parameterised the along-flowline climatic temperature sensitivities of these
808 glaciers using the method proposed by Shea and Moore (2010) and presented the results in the
809 context of several available distributed on-glacier datasets ~~to date~~. The key findings of this work
810 are:

- 811
812 1. For our Tibetan case study, on-glacier air temperatures at short flowline distances ~~are~~
813 more climate sensitive display a high temperature sensitivity (i.e. demonstrate a
814 relationship with off-glacier air temperature that is ~~closer~~ close to 1). We therefore
815 confirm earlier evidence regarding the high temperature sensitivity of high elevation,
816 small glaciers (flowline distances < 1000 m) to external climate, and thus future warming.
- 817 2. The largest offsets differences between observed on-glacier and estimated off-glacier air
818 temperatures are found for the warmest off-glacier hours, during drier, clear sky
819 conditions of the summer monsoon period.
- 820 3. Above the established onset of the katabatic boundary layer, climatic temperature
821 sensitivity to ambient temperature decreases rapidly up to ~2000-3000 m along the
822 glacier flowline. Beyond this distance, both the Tibetan glaciers and other datasets of the
823 literature show a slower decrease of climatic temperature sensitivity.

- 824 4. A parameterisation for the ~~climatic~~temperature sensitivity of the Tibetan study glaciers
825 implies a ~~smaller~~similar boundary layer effect ~~than~~compared to the existing
826 parameterisation of Shea and Moore (2010). The climatology of a given region may
827 influence the magnitude of the glacier's ~~climatic~~temperature sensitivity, though no clear
828 relationships with the climatology of the glacier sites are found, thus suggesting the
829 stronger role of local meteorological or topographic effects on the along-flowline pattern
830 of T_a variability.
- 831 5. The terminus of some glaciers ~~remains~~ associated with other warm air processes,
832 possibly due to boundary layer divergence, warm up-valley winds, large glacier slope
833 changes or debris cover/valley heating. We find that these effects are evident only beyond
834 ~70% of the total glacier flowline distance, although further work is required to explain
835 this behaviour. A better understanding of temperature variability for this lower 30% is
836 highly important as ~~most of the summer melting will occur for this sector~~part of the
837 glacier- is most affected by ablation.

838
839 In summarising the findings from all available distributed on-glacier datasets to date, we identify
840 some key directions for future work on this subject. This includes comparing local influences of
841 glacier size and micro-meteorology and standardising measurement practices, where possible, to
842 aidenable the ~~conclusions for construction of~~ a generalised model ~~off~~or on-glacier air temperature
843 estimation.
844

845 Acknowledgements

846 Funding for the instrumentation of the Parlung catchment was provided by NSFC project
847 (91647205 and 4191101270) and Newton Advanced Fellowship (NA170325). This project has
848 received funding from the European Research Council (ERC) under the European Union's
849 Horizon 2020 research and innovation programme grant agreement No 772751, RAVEN, "Rapid
850 mass losses of debris covered glaciers in High Mountain Asia". Á. Ayala acknowledges support
851 from a FONDECYT project (number 3190732) and C. Bravo from the ANID Becas Chile PhD
852 scholarship program. ~~F. Pellicciotti acknowledges an ERC Consolidator Grant: 'RAVEN' (Rapid~~
853 ~~mass loss of debris covered glaciers in High Mountain Asia, grant agreement no. 772751).~~ The
854 authors kindly acknowledge the sharing of global datasets or parameters provided to aid this
855 analysis, explicitly M. Nolan (McCall Glacier), J. Pomeroy, D. Pradhananga and the Global Water
856 Futures Programme (Peyto Glacier), P. Smeets and IMAU, Utrecht (Pasterze Glacier), DGA,
857 Chile (Universidad Glacier and Greve Glacier) and L. Carturan (AVDM, Italy). E. Ludewig is
858 thanked for the provision of off-glacier temperature records at Sonnblick station, Austria.
859 Additionally we recognise the hard work involved in obtaining and sharing all of the datasets
860 acquired and the acknowledgements of those works. Scientific editor T. Sauter, L. Carturan and
861 one anonymous reviewer are thanked for their insightful and constructive comments that have
862 improved the quality of the manuscript.

863 Author contributions

864 TES and WY discussed and designed the research plan with Parlung data provided by WY and
865 CZ. Additional data and analysis was provided by AA and CB. TES wrote the manuscript with
866 scientific input from all co-authors.

867 Data availability

868 Calculated flowlines and ~~climatic~~temperature sensitivities are available at the following Zenodo
869 repository: <http://doi.org/10.5281/zenodo.3937777><http://doi.org/10.5281/zenodo.3937777>

870 Competing Interests

871 The authors declare that they have no conflicting interests.

873 **References**

- 874 ASF DAAC: ALOS PALSAR_Radiometric_Terrain_Corrected_low_res; Includes Material ©
 875 JAXA/METI 2007. Accessed through ASF DAAC 20th March, 2020.
 876 DOI: 10.5067/JBYK3J6HFSVF, 2020
- 877 Arnold, N. S., Rees, W. G., Hodson, A. J., & Kohler, J.: Topographic controls on the surface
 878 energy balance of a high Arctic valley glacier. *J. Geophys. Res.*, 111(F2), F02011.
 879 <https://doi.org/10.1029/2005JF000426>, 2006
- 880 Ayala, A., Pellicciotti, F., & Shea, J.: Modeling 2m air temperatures over mountain glaciers:
 881 Exploring the influence of katabatic cooling and external warming. *J. Geophys. Res: Atmos*, 120,
 882 1–19. <https://doi.org/10.1002/2015JD023137> , 2015
- 883 Betts, A. K., Chan, D. Z., & Desjardins, R. L.: Near-Surface Biases in ERA5 Over the Canadian
 884 Prairies. *Front. Environ. Sci.*, 7. <https://doi.org/10.3389/fenvs.2019.00129> , 2019
- 885 Bonekamp, P. N. J., Heerwaarden, C. C. Van, Steiner, J. F., & Immerzeel, W. W.: Using 3D
 886 turbulence-resolving simulations to understand the impact of surface properties on the energy
 887 balance of a debris-covered glacier. *Cryosph.*, 14, 1611–1632. [https://doi.org/10.5194/tc-14-1611-](https://doi.org/10.5194/tc-14-1611-2020)
 888 [2020](https://doi.org/10.5194/tc-14-1611-2020) , 2020
- 889 Bravo, C., Quincey, D. J., Ross, A. N., Rivera, A., Brock, B. W., Miles, E., & Silva, A.: Air
 890 Temperature Characteristics , Distribution , and Impact on Modeled Ablation for the South
 891 Patagonia Ice field. *J. Geophys. Res: Atmos*, 124, 907–925.
 892 <https://doi.org/10.1029/2018JD028857> , ~~2019~~2019a
- 893 [Bravo, C., Bozkurt, D., Gonzalez-reyes, Á., Quincey, D. J., Ross, A. N., Farias-Barahona, D., &](https://doi.org/10.3389/fenvs.2019.00030)
 894 [Rojas, M.: Assessing Snow Accumulation Patterns and Changes on the Patagonian Icefields.](https://doi.org/10.3389/fenvs.2019.00030)
 895 [Frontiers in Environmental Science, 7\(March\), 1–18. https://doi.org/10.3389/fenvs.2019.00030,](https://doi.org/10.3389/fenvs.2019.00030)
 896 [2019b](https://doi.org/10.3389/fenvs.2019.00030)
- 897 Bravo, C., Lorlaux, T., Rivera, A., & Brock, B. W.: Assessing glacier melt contribution to
 898 streamflow at Universidad Glacier, central Andes of Chile. *Hydrol. Earth Syst. Sci.*, 21, 3249–
 899 3266. <https://doi.org/10.5194/hess-21-3249-2017> , 2017
- 900 Brock, B. W., Mihalcea, C., Kirkbride, M. P., Diolaiuti, G., Cutler, M. E. J., & Smiraglia, C.:
 901 Meteorology and surface energy fluxes in the 2005–2007 ablation seasons at the Miage debris-
 902 covered glacier, Mont Blanc Massif, Italian Alps. *J. Geophys. Res.*, 115, D09106.
 903 <https://doi.org/10.1029/2009JD013224> , 2010
- 904 Caidong, C., & Sorteberg, A.: Modelled mass balance of Xibu glacier, Tibetan Plateau: Sensitivity
 905 to climate change. *J. Glaciol.*, 56(196), 235–248. <https://doi.org/10.3189/002214310791968467> ,
 906 2010
- 907 Carturan, L., Cazorzi, F., De Blasi, F., & Dalla Fontana, G.: Air temperature variability over three
 908 glaciers in the Ortles–Cevedale (Italian Alps): effects of glacier fragmentation, comparison of
 909 calculation methods, and impacts on mass balance modeling. *Cryosph.*, 9(3), 1129–1146.
 910 <https://doi.org/10.5194/tc-9-1129-2015> , 2015
- 911 Copernicus Climate Change Service (C3S): ERA5: Fifth generation of ECMWF atmospheric
 912 reanalyses of the global climate . Copernicus Climate Change Service Climate Data Store (CDS),
 913 Available at: <https://cds.climate.copernicus.eu/cdsapp#!/home>. Accessed 05/05/2020 , 2017

- 914 Ding, B., Yang, K., Yang, W., He, X., Chen, Y., Lazhu, ... Yao, T.: Development of a Water and
915 Enthalpy Budget-based Glacier mass balance Model (WEB-GM) and its preliminary validation.
916 *Water Resour. Res.*, 53(4), 3146–3178. <https://doi.org/10.1002/2016WR018865> , 2017
- 917 Gabbi, J., Carenzo, M., Pellicciotti, F., Bauder, A., & Funk, M.: A comparison of empirical and
918 physically based glacier surface melt models for long-term simulations of glacier response. *J.*
919 *Glaciol*, 60(224), 1140–1154. <https://doi.org/10.3189/2014JoG14J011> , 2014
- 920 Gardner, A. S., Sharp, M. J., Koerner, R. M., Labine, C., Boon, S., Marshall, S. J., ... Lewis, D.:
921 Near-Surface Temperature Lapse Rates over Arctic Glaciers and Their Implications for
922 Temperature Downscaling. *J. Clim.*, 22(16), 4281–4298.
923 <https://doi.org/10.1175/2009JCLI2845.1>, 2009
- 924 Georges, C., & Kaser, G.: Ventilated and unventilated air temperature measurements for glacier-
925 climate studies on a tropical high mountain site. *J. Geophys. Res.*, 107(D24), 4775.
926 <https://doi.org/10.1029/2002JD002503> , 2002
- 927 Greuell, W., & Böhm, R.: 2 m temperatures along melting mid-latitude glaciers , and implications
928 for the sensitivity of the mass balance to variations in temperature. *J. Glaciol*, 44(146), 9–20. ,
929 1998
- 930 Greuell, W., Knap, W. H., & Smeets, P. C.: Elevational changes in meteorological variables along
931 a midlatitude glacier during summer. *J. Geophys. Res.*, 102(D22), 25941.
932 <https://doi.org/10.1029/97JD02083> , 1997
- 933 Hannah, D. M., Gurnell, A. M., & McGregor, G. R.: Spatio-temporal variation in microclimate,
934 the surface energy balance and ablation over a cirque glacier. *Int. J. Climatol.*, 20(7), 733–758.
935 [https://doi.org/10.1002/1097-0088\(20000615\)20:7](https://doi.org/10.1002/1097-0088(20000615)20:7) , 2000
- 936 Heynen, M., Miles, E., Ragetti, S., Buri, P., Immerzeel, W., & Pellicciotti, F.: Air temperature
937 variability in a high elevation Himalayan catchment. *Ann. Glaciol.*, 57(71),
938 <https://doi.org/10.3189/2016AoG71A076> , 2016
- 939 Huintjes, E., Sauter, T., Schröter, B., Maussion, F., Yang, W., Kropáček, J., ... Schneider, C.:
940 Evaluation of a Coupled Snow and Energy Balance Model for Zhadang Glacier, Tibetan Plateau,
941 Using Glaciological Measurements and Time-Lapse Photography. *Arctic, Antarct. Alp. Res.*,
942 47(3), 573–590. <https://doi.org/10.1657/AAAR0014-073> , 2015
- 943 Immerzeel, W. W., Petersen, L., Ragetti, S., & Pellicciotti, F.: The importance of observed
944 gradients of air temperature and precipitation for modeling runoff from a glacierized watershed.
945 *Water Resour. Res.*, 50, 2212–2226. <https://doi.org/10.1002/2013WR014506>. , 2014
- 946 Jiskoot, H., & Mueller, M. S.: Glacier fragmentation effects on surface energy balance and runoff:
947 field measurements and distributed modelling. *Hydrol. Process.*, 26(12), 1861–1875.
948 <https://doi.org/10.1002/hyp.9288> , 2012
- 949 Jobst, A. M., Kingston, D. G., Cullen, N. J., & Sirguey, P.: Combining thin-plate spline
950 interpolation with a lapse rate model to produce daily air temperature estimates in a data-sparse
951 alpine catchment. *Int. J. Climatol.*. <https://doi.org/10.1002/joc.4699> , 2016
- 952 Marshall, S. J., Sharp, M. J., Burgess, D. O., & Anslow, F. S.: Near-surface-temperature lapse
953 rates on the Prince of Wales Icefield, Ellesmere Island, Canada: implications for regional
954 downscaling of temperature. *Int. J. Climatol.*, 27, 1549–1555. <https://doi.org/10.1002/joc> , 2007

- 955 Maurer, J. M., Schaefer, J. M., Rupper, S., & Corley, A.: Acceleration of ice loss across the
956 Himalayas over the past 40 years. *Sci. Adv.*, 5, 1–12., 2019
- 957 Minder, J. R., Mote, P. W., & Lundquist, J. D.: Surface temperature lapse rates over complex
958 terrain: Lessons from the Cascade Mountains. *J. Geophys. Res.*, 115(D14), D14122.
959 <https://doi.org/10.1029/2009JD013493> , 2010
- 960 Mölg, T., Maussion, F., Yang, W., & Scherer, D.: The footprint of Asian monsoon dynamics in
961 the mass and energy balance of a Tibetan glacier. *Cryosph.*, 6(6), 1445–1461.
962 <https://doi.org/10.5194/tc-6-1445-2012> , 2012
- 963 Munro, D. S.: Linking the weather to glacier hydrology and mass balance at Peyto glacier. *Peyto*
964 *Glacier: One Century of Science*. National Hydrology Research Institute Science Report #8. ,
965 2006
- 966 Munro, D. S., & Marosz-Wantuch, M.: Modeling Ablation on Place Glacier, British Columbia,
967 from Glacier and Off-glacier Data Sets. *Arctic, Antarct. Alp. Res.*, 41(2), 246–256.
968 <https://doi.org/10.1657/1938-4246-41.2.246> , 2009
- 969 Nolin, A. W., Phillippe, J., Jefferson, A., & Lewis, S. L.: Present-day and future contributions of
970 glacier runoff to summertime flows in a Pacific Northwest watershed: Implications for water
971 resources. *Water Resour. Res.*, 46(12). <https://doi.org/10.1029/2009WR008968> , 2010
- 972 Oerlemans, B. J., & Grisogono, B.: Glacier winds and parameterisation of the related surface heat
973 fluxes. *Tellus*, 54, 440–452. , 2002
- 974 Oerlemans, J.: *The microclimate of valley glaciers*. Utrecht Publishing and Archiving Services,
975 Universiteitsbibliotheek, Utrecht. , 2010
- 976 Oerlemans, J.: *Glaciers and Climate Change*. , 2001
- 977 Pellicciotti, F., Helbing, J., Rivera, A., Favier, V., Corripio, J. G., Araos, J., ... Carenzo, M.: A
978 study of the energy balance and melt regime on Juncal Norte Glacier , semi-arid Andes of central
979 Chile , using melt models of different complexity. *Hydrol. Process.*, 22, 3980–3997.
980 <https://doi.org/10.1002/hyp> , 2008
- 981 Petersen, L., & Pellicciotti, F.: Spatial and temporal variability of air temperature on a melting
982 glacier: Atmospheric controls, extrapolation methods and their effect on melt modeling, Juncal
983 Norte Glacier, Chile. *J. Geophys. Res.*, 116(D23), D23109.
984 <https://doi.org/10.1029/2011JD015842> , 2011
- 985 Petersen, L., Pellicciotti, F., Juszak, I., Carenzo, M., & Brock, B. W.: Suitability of a constant air
986 temperature lapse rate over an Alpine glacier: testing the Greuell and Böhm model as an
987 alternative. *Ann. Glaciol.*, 54(63), 120–130. <https://doi.org/10.3189/2013AoG63A477> , 2013
- 988 [Pradhananga, D., Pomeroy, J. W., Aubry-Wake, C., Munro, D. S., Shea, J., Demuth, M. N., Kirat,](#)
989 [N. H., Menounos, B., and Mukherjee, K.: Hydrometeorological, glaciological and geospatial](#)
990 [research data from the Peyto Glacier Research Basin in the Canadian Rockies, *Earth Syst. Sci.*](#)
991 [Data Discuss.](#), <https://doi.org/10.5194/essd-2020-219>, in review, 2020.
- 992 Ragettli, S., Immerzeel, W. W., & Pellicciotti, F.: Contrasting climate change impact on river
993 flows from high-altitude catchments in the Himalayan and Andes Mountains. *Proc. Natl. Acad.*
994 *Sci.*, 113(33). <https://doi.org/10.1073/pnas.1606526113> , 2016

- 995 Rets, E. P., Popovnin, V. V., Toropov, P. A., Smirnov, A. M., Tokarev, I. V., Chizhova, J. N., ...
996 Kireeva, M. B.: Djankuat glacier station in the North Caucasus , Russia : a database of
997 glaciological , hydrological , and meteorological observations and stable isotope sampling results
998 during 2007 – 2017. *Earth Syst. Sci. Data*, 1463–1481.
999 <https://doi.org/https://doi.org/10.5194/essd-11-1463-2019> , 2019
- 1000 Sauter, T., & Galos, S. P.: Effects of local advection on the spatial sensible heat flux variation on
1001 a mountain glacier. *Cryosph.*, 10, 2887–2905. <https://doi.org/10.5194/tc-10-2887-2016> , 2016
- 1002 Schwanghart, W., Kuhn, N, J.: TopoToolbox: A set of Matlab functions for topographic analysis,
1003 *Environmental Modelling & Software*, 25 (6), 770-781.
1004 <https://doi.org/10.1016/j.envsoft.2009.12.002> . , 2010
- 1005 Shaw, T. E., Brock, B. W., Ayala, A., Rutter, N., & Pellicciotti, F.: Centreline and cross-glacier
1006 air temperature variability on an Alpine glacier: assessing temperature distribution methods and
1007 their influence on melt model calculations. *J. Glaciol.*, 1–16. <https://doi.org/10.1017/jog.2017.65>
1008 , 2017
- 1009 Shaw, T., Brock, B., Fyffe, C., Pellicciotti, F., Rutter, N., & Diotri, F.: Air temperature
1010 distribution and energy balance modelling of a debris-covered glacier. *J. Glaciol.*, 62(231), 185–
1011 198. <https://doi.org/10.1017/jog.2016.31> , 2016
- 1012 Shea, J. M., & Moore, R. D.: Prediction of spatially distributed regional-scale fields of air
1013 temperature and vapor pressure over mountain glaciers. *J. Geophys. Res.*, 115(D23), D23107.
1014 <https://doi.org/10.1029/2010JD014351> , 2010
- 1015 Steiner, J. F. and Pellicciotti, F.: Variability of air temperature over a debris-covered glacier in
1016 the Nepalese Himalaya, *Ann. Glaciol.*, 57(71), 295–307, doi:10.3189/2016AoG71A066, 2016.
- 1017 Strasser, U., Corripio, J. G., Pellicciotti, F., Burlando, P., Brock, B. W., & Funk, M.: Spatial and
1018 temporal variability of meteorological variables at Haut Glacier d’Arolla (Switzerland) during the
1019 ablation season 2001: Measurements and simulations. *J. Geophys. Res.*, 109, D03103.
1020 <https://doi.org/10.1029/2003JD003973> , 2004
- 1021 Troxler, P., Ayala, Á., Shaw, T. E., Nolan, M., Brock, B. W., & Pellicciotti, F.: Modelling spatial
1022 patterns of near-surface air temperature over a decade of melt seasons on McCall Glacier, Alaska.
1023 *J. Glaciol.*, 1–15. <https://doi.org/https://doi.org/10.1017/jog.2020.12> , 2020
- 1024 van de Wal, R. S. W., Oerlemans, J., & Van Der Hage, J. C.: A study of ablation variations on
1025 the tongue of Hintereisferner, Austrian Alps. *J. Glaciol.*, 38(130), 319–324. , 1992
- 1026 van den Broeke, M. R.: Momentum , Heat , and Moisture Budgets of the Katabatic Wind Layer
1027 over a Midlatitude Glacier in Summer. *J. Appl. Meteorol.*, 36(1987), 763–774. , 1997
- 1028 Wang, R., Liu, S., Shanguan, D., Radić, V., & Y, Z.: Spatial Heterogeneity in Glacier Mass-
1029 Balance. *Water*, 11(776), 1–21. <https://doi.org/doi:10.3390/w11040776> , 2019
- 1030 Yang, W., Guo, X., Yao, T., Yang, K., Zhao, L., Li, S., & Zhu, M.: Summertime surface energy
1031 budget and ablation modeling in the ablation zone of a maritime Tibetan glacier. *J. Geophys. Res.*
1032 *Atmos*, 116(14), 1–11. <https://doi.org/10.1029/2010JD015183> , 2011

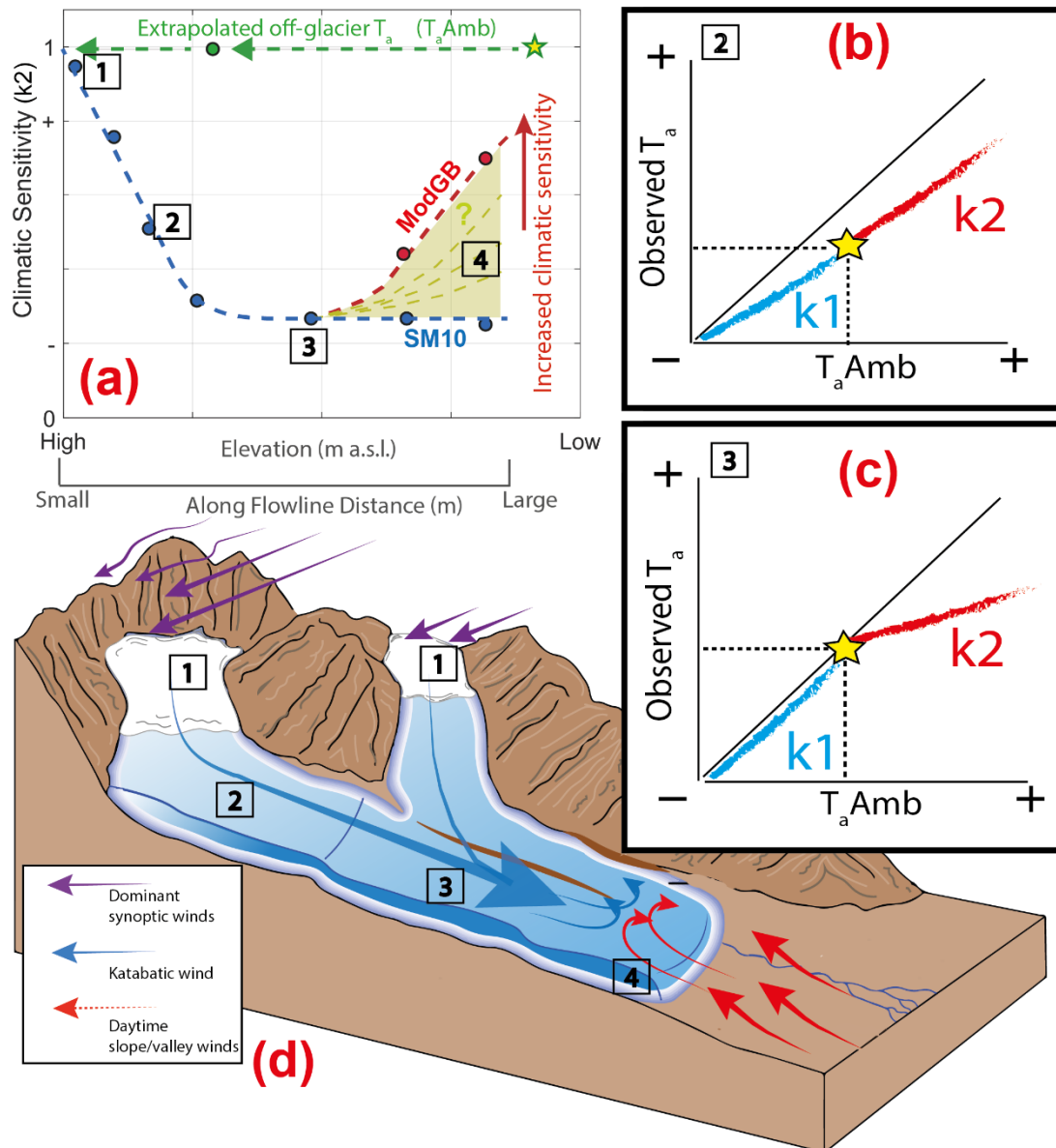
1033 Yang, W., Yao, T., Guo, X., Zhu, M., Li, S., & Kattel, D. B.: Mass balance of a maritime glacier
1034 on the southeast Tibetan Plateau and its ~~climate~~temperature sensitivity. J. Geophys. Res. Atmos,
1035 118(17), 9579–9594. <https://doi.org/10.1002/jgrd.50760> , 2013

1036 Zhao, L., Tian, L., Zwinger, T., Ding, R., Zong, J., Ye, Q., & Moore, J. C.: Numerical simulations
1037 of Gurenhekou glacier on the Tibetan Plateau. J. Glaciol, 60(219), 71–82.
1038 <https://doi.org/10.3189/2014JoG13J126> , 2014

1039 Zhu, M., Yao, T., Yang, W., Maussion, F., Huintjes, E., & Li, S.: Energy- and mass-balance
1040 comparison between Zhadang and Parlung No. 4 glaciers on the Tibetan Plateau. J. Glaciol,
1041 61(227), 595–607. <https://doi.org/10.3189/2015JoG14J206> , ~~2015~~201

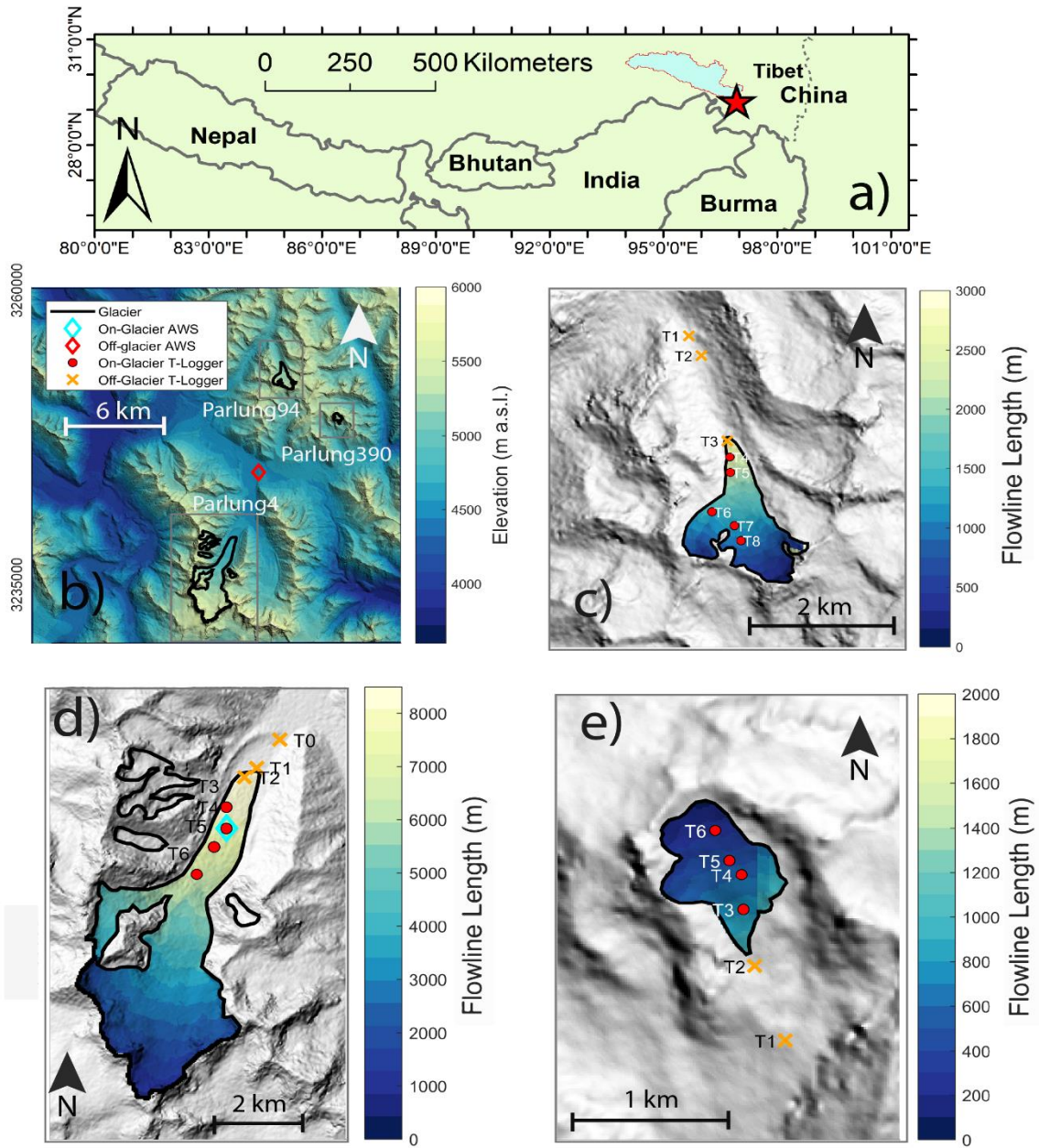
1042
1043
1044
1045
1046
1047
1048
1049
1050
1051
1052
1053
1054
1055
1056
1057
1058
1059
1060
1061
1062
1063
1064
1065
1066

Figures



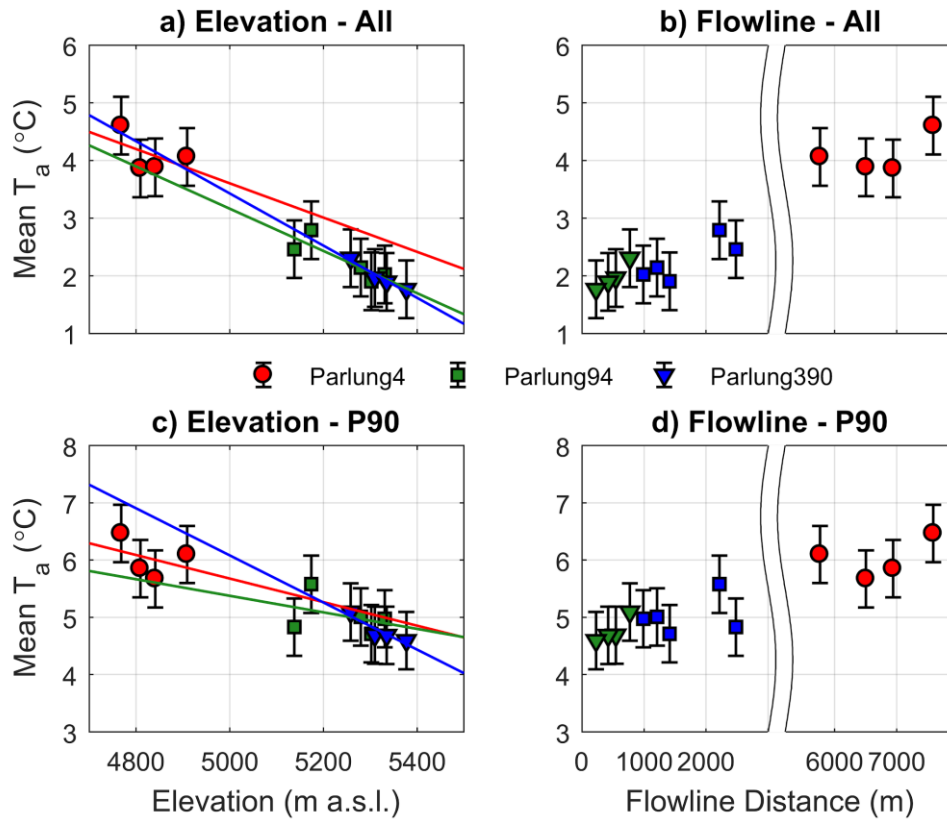
1067
 1068
 1069
 1070
 1071
 1072
 1073
 1074
 1075
 1076
 1077
 1078
 1079
 1080

Figure 1: A schematic diagram to describe the climatic sensitivity of on-glacier air temperature (T_a) to the extrapolated ambient temperature ($T_{a,Amb}$) at given elevations/flowline distances on a mountain glacier. Points 1-4 indicate locations of interest in the context of the current science for this topic that are linked between panels. Panel (a) indicates the along-flowline 'k2' climatic sensitivities to $T_{a,Amb}$, considering down-glacier decrease in sensitivities and the observed differences in the models of SM10 and ModGB for glacier termini (see text). While ModGB does not explicitly include the k2 parameter, its approach is similar to considering an increasing climatic sensitivity to $T_{a,Amb}$ (see Ayala et al., 2015). The green line in panel (a) indicates the local off-glacier lapse rate to estimate $T_{a,Amb}$ using off-glacier observations at varying elevations (green dot). Panels (b) and (c) represent the differences of k1 and k2 sensitivities observed in the data at different theoretical locations on the glacier (see Figure 5, for examples on Parlung glaciers), the latter of which shows the theoretical parameterisation presented by Shea and Moore (2010). Panel (d) represents an idealised case of katabatic and valley/synoptic wind interactions that potentially dictate the along-flowline structure of on-glacier climatic sensitivity and thus T_a estimation.



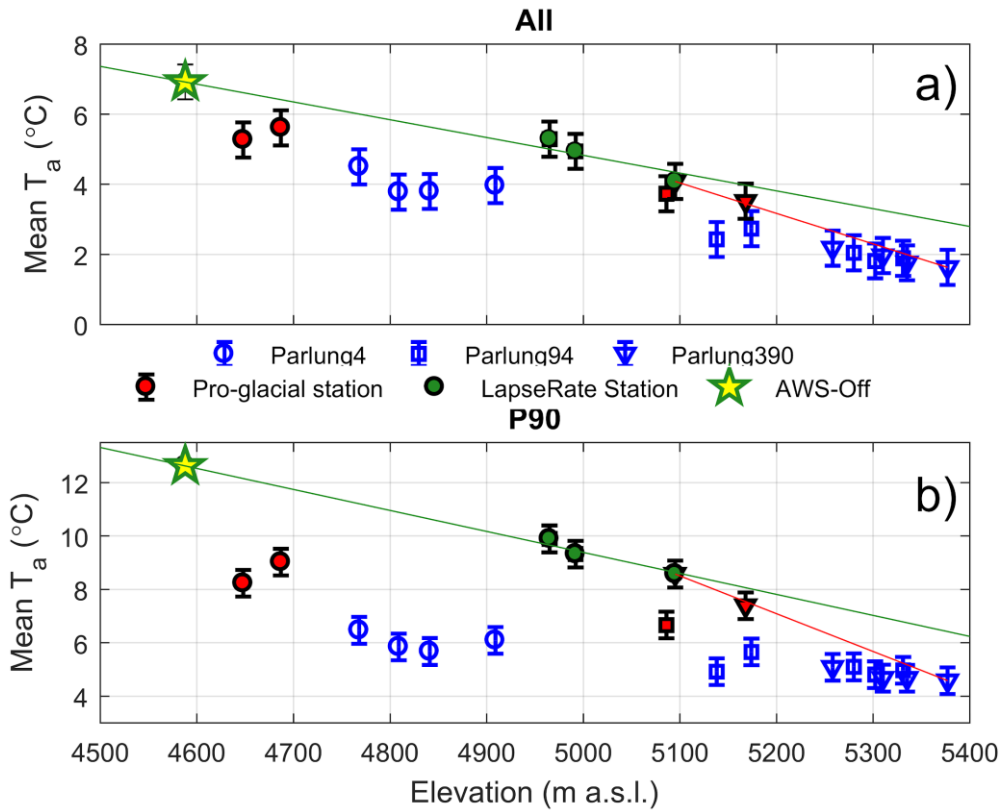
1081
 1082 *Figure 2: The location of Parlung catchment in Tibet (a) and a map of the Parlung catchment (b) with the*
 1083 *study glaciers, Parlung 94 (c), Parlung 4 (d) and Parlung 390 (e). Off glacier and on glacier AWS and T-*
 1084 *Logger locations are shown (without glacier number suffix). (a) shows the elevation of the catchment (DEM*
 1085 *source: Alos Palsar) and (b-d) show the calculated flowline distances based upon TopoToolbox (scales*
 1086 *vary).*

1087
 1088
 1089



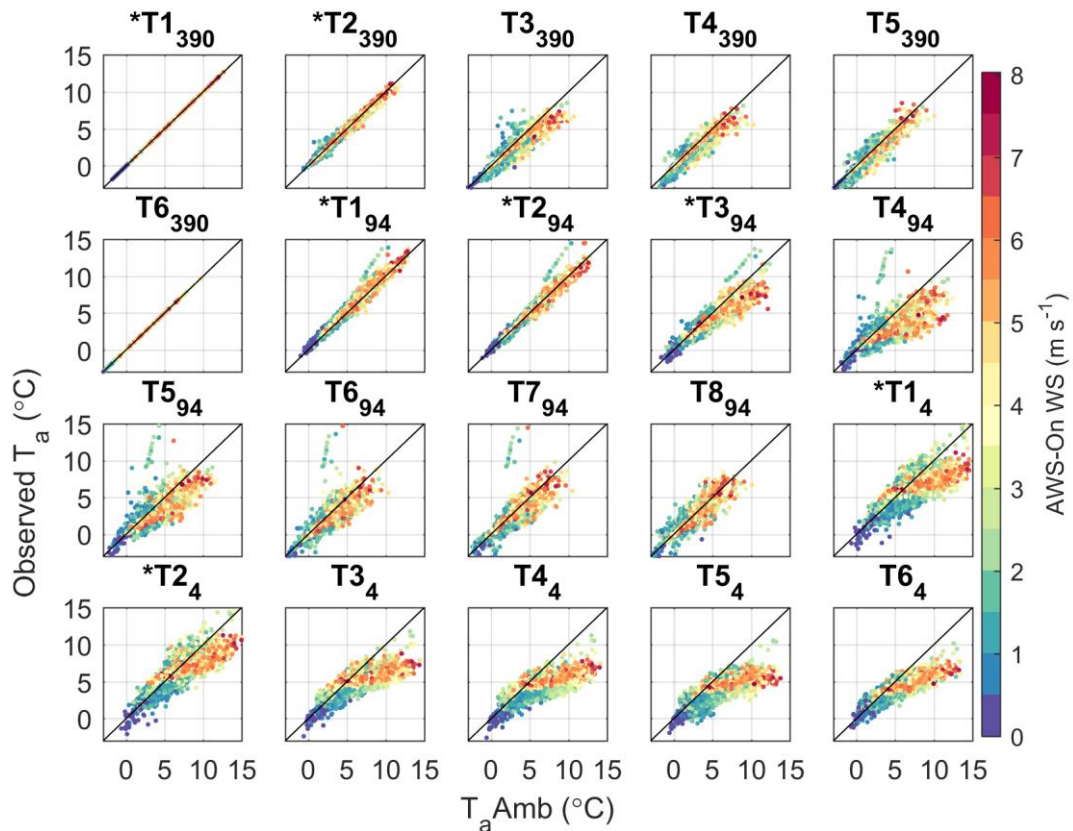
1090
 1091
 1092
 1093
 1094
 1095

Figure 3: The elevation-mean T_a and uncertainty (errorbar) for (a) all hours and (c) P90 hours ($n = 312$). Panels (b) and (d) are the equivalent plots against flowline distance. Coloured lines show the linear fit against elevation ('lapse rate') to each glacier. An x axis scale break is used in (b) and (d) for clarity.



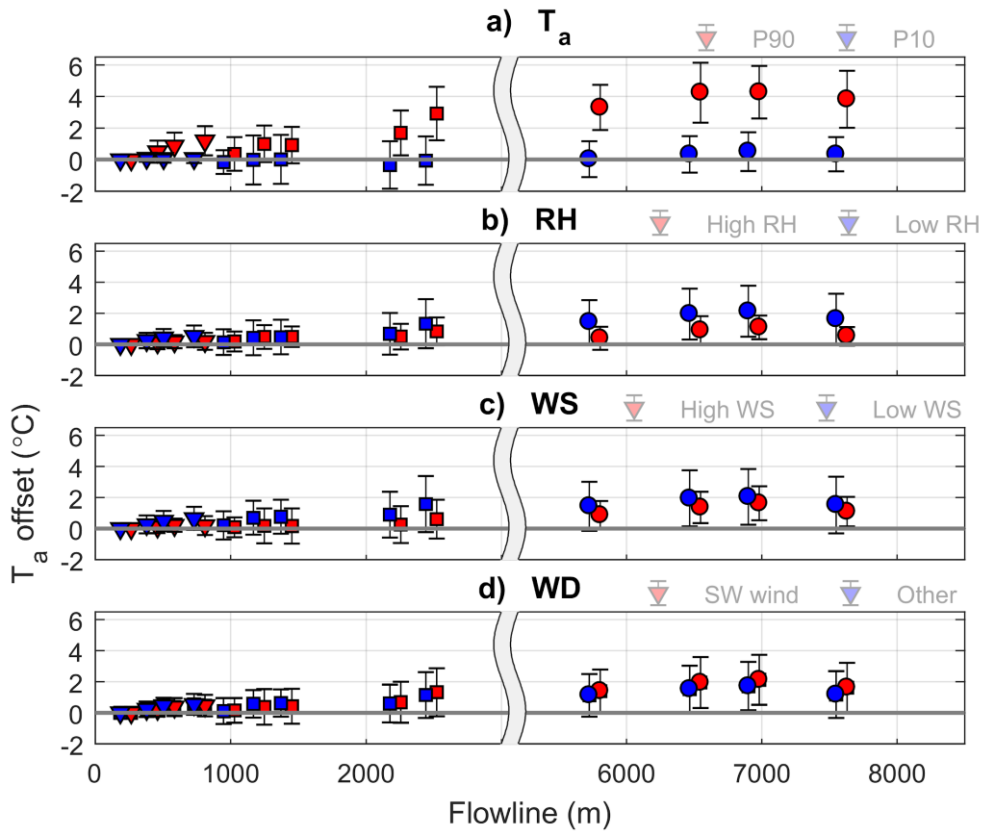
1096
 1097
 1098
 1099
 1100
 1101
 1102

Figure 4: The mean T_a against elevation for all hours (a) and P90 hours (b), where blue markers are on-glacier T Loggers, red markers are pro-glacial T Loggers and green circles denote off-glacier T Loggers used to construct an hourly variable 'catchment lapse rate' (green line), extrapolated from AWS_Off (star). The red line indicates the piecewise lapse rate above the elevation of T1_390 to lapse T_a to the top of the flowline. A 0.5°C uncertainty is shown by the errorbar for each station (not applied to the lapse rate for neatness).



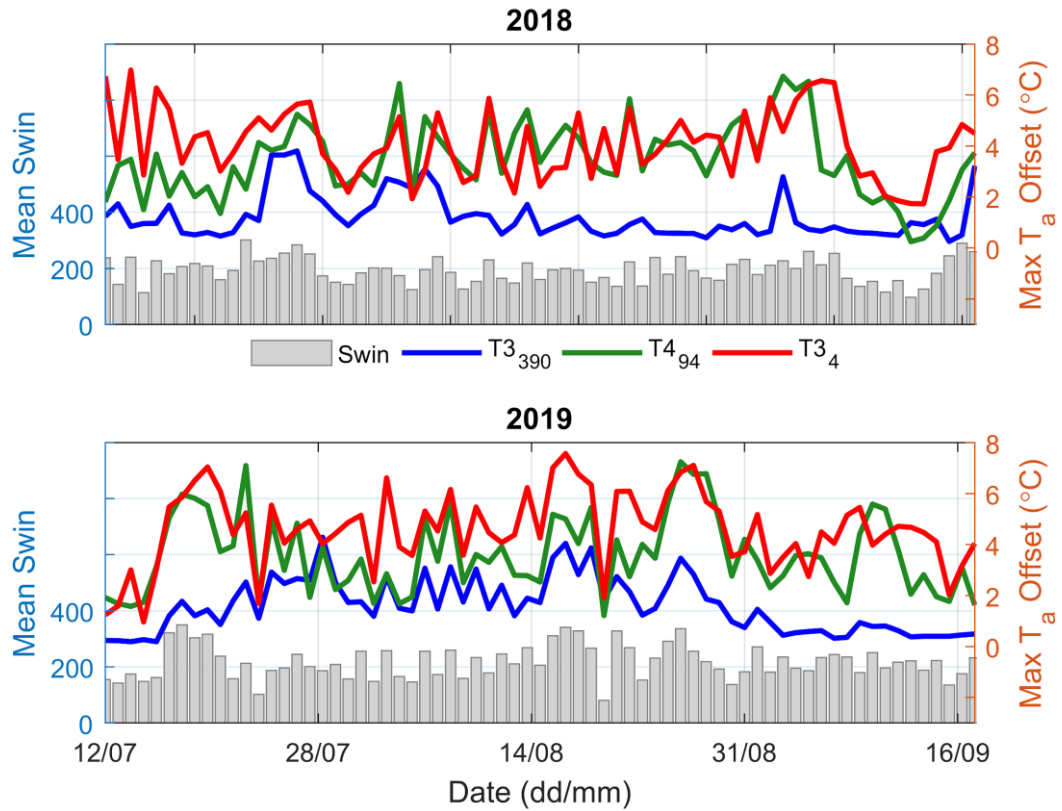
1103
 1104
 1105
 1106
 1107
 1108
 1109
 1110
 1111
 1112

*Figure 5: Estimated (T_a Amb) vs Observed T_a at each T-Logger location (including off glacier T-Loggers). Individual hourly values are coloured by the observed wind speeds at AWS-On (Parlung4). No on glacier wind speed data exist for Parlung94 and Parlung390, so the coloured markers are only assumed for those glaciers from the parlung4 wind speed data. * denotes stations that are off glacier.*



1113
 1114
 1115
 1116
 1117
 1118
 1119
 1120
 1121

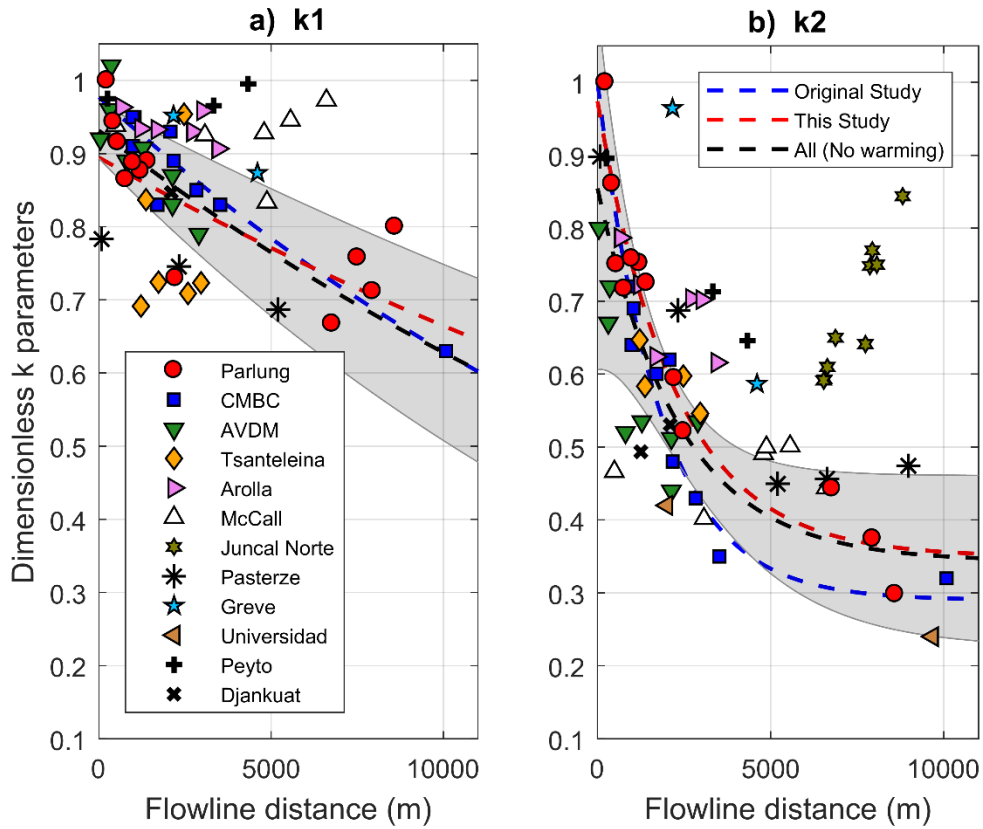
Figure 6: The mean and standard deviation (error bars) of hourly T_a bias offsets (estimated - observed) along the glacier flowline. Each panel depicts hourly grouping by (a) off glacier T_a at AWS_Off (P90 is $\geq 10.5^{\circ}$ C and P10 is $\leq 3.5^{\circ}$ C), (b) off glacier RH at AWS_Off (high is $> 90\%$ and low is $< 70\%$), (c) wind speed from ERA5 (high $\Rightarrow 2.5 \text{ m s}^{-1}$ and low $\Rightarrow 0.7 \text{ m s}^{-1}$) and (d) dominant wind direction from ERA5 (Southwest wind direction is considered as $180-270^{\circ}$). Marker shapes show the different glaciers, as in Figure 3 and 4.



1122

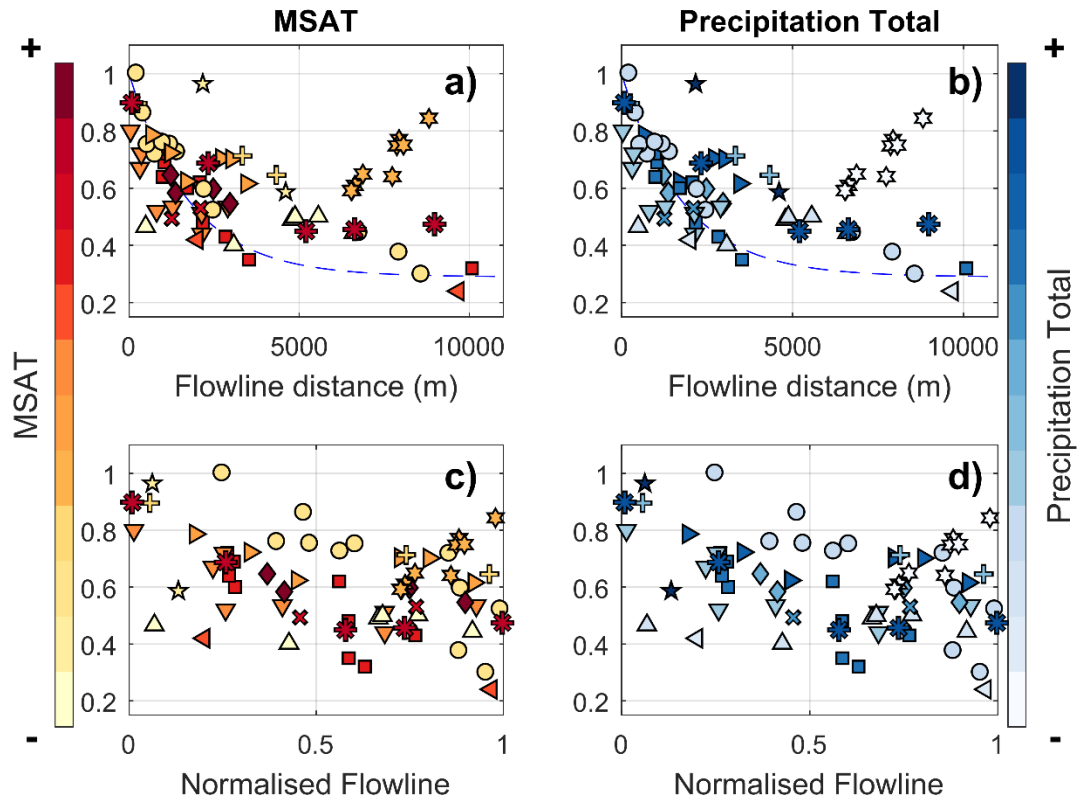
1123 *Figure 7: Maximum daily T_a offsets (estimated—observed) at the most distant along flowline T Loggers on*
 1124 *each glacier for (top) and 2019 (bottom). Mean daily incoming shortwave radiation at AWS_Off is shown*
 1125 *by the grey bars.*

1126



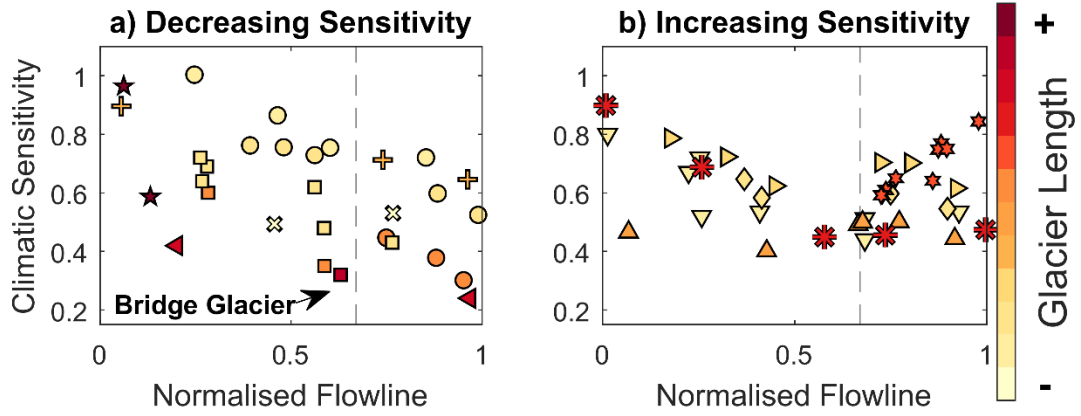
1127

1128 *Figure 8: The calculated k_1 and k_2 sensitivities as a function of the flowline distance of each observation*
 1129 *on the Parlung glaciers (red circles) and other, global datasets (Table 2). The dashed blue and red lines*
 1130 *show the fitted exponential parameterisation of Shea and Moore (2010) and this study, respectively. The*
 1131 *dashed black line and shaded area denotes the equivalent parameterisation for all observations where a*
 1132 *large increase in sensitivity on the glacier terminus ('warming effect') is absent (explicitly excluding data*
 1133 *from McCall, Juncal Norte and Djankuat). The shaded area represents the 95% confidence interval of this*
 1134 *fit line.*



1135 *Figure 9: The k_2 sensitivities as a function of flowline distance (top) and a normalized distance, considering*
 1136 *the total flowline distance for the year of study (bottom). The individual glaciers of grouped studies*
 1137 *(Parlung, CMBC and AVDM) are separated and normalized by the individual glacier length (symbols as*
 1138 *in Figure 8). Glaciers are coloured by rankings of the mean summer air temperatures (MSAT—left) and*
 1139 *precipitation total (PT—right). The original parameterisation is retained in the top panels.*
 1140

1141
 1142
 1143
 1144
 1145
 1146
 1147
 1148
 1149
 1150
 1151
 1152
 1153
 1154



1155
 1156
 1157
 1158
 1159
 1160
 1161
 1162
 1163
 1164
 1165
 1166
 1167
 1168
 1169
 1170
 1171
 1172
 1173
 1174
 1175
 1176
 1177
 1178
 1179
 1180
 1181
 1182
 1183
 1184
 1185
 1186
 1187

Figure 10: The k_2 sensitivity along the normalized flowline compared to total glacier length (colour bar) and subjectively grouped by the evidence of a relative warming effect (increasing climatic sensitivity) toward the glacier terminus.

1188
 1189
 1190
 1191

Tables

~~Table 1: Details of each AWS/T-Logger station used in this analysis including the calculated flowline distances.~~

Station	Latitude	Longitude	Elevation (m a.s.l.)	Flowline (m)	on/off glacier
AWS_Off	29.314	96.955	4588	-	off
AWS_On	29.500	97.009	4649	-	off
T1₂₀₀	29.348	97.022	5095	-	off
T2₂₀₀	29.352	97.020	5168	-	off
T3₂₀₀	29.354	97.020	5258	770	on
T4₂₀₀	29.356	97.020	5310	544	on
T5₂₀₀	29.357	97.019	5335	420	on
T6₂₀₀	29.359	97.018	5377	224	on
T1₀₄	29.621	97.218	4965	-	off
T2₀₄	29.417	96.99	4992	-	off
T3₀₄	29.635	96.975	5086	-	off
T4₀₄	29.596	97.065	5138	2481	on
T5₀₄	29.56	97.067	5174	2215	on
T6₀₄	29.466	97.023	5302	1411	on
T7₀₄	29.434	97.080	5280	1208	on
T8₀₄	29.399	97.097	5321	988	on
T1₄	29.271	96.968	4690	-	off
T2₄	29.368	96.935	4769	-	off
T3₄	29.298	97.168	4809	8589	on
T4₄	29.298	97.168	4809	7940	on
T5₄	29.496	97.126	4841	7505	on
T6₄	29.403	97.068	4909	6765	on

1192
 1193
 1194

 1195

 1196

 1197

 1198

 1199

 1200

 1201

 1202
 1203

~~Table 2: The details of each site where distributed on glacier air temperatures are available. Elevation~~

1204
1205

ranges and mean summer air temperatures (MSAT) are reported for the year of investigation. Precipitation totals (mm—PT) was obtained upon cited literature.

Site	Lat	Lon	Year(s)	Elevation	MSA T	PT	T_a Data Reference
				m.a.s.l.	°C	mm	
Parlung (Tibet)	29.24	96.93	2018-2019	4600-5800	2.19	679	This Study
CMBC (Canada)	50.32	-122.48	2006-2008	1375-2898	10.29	1113	Shea and Moore (2010)
AVDM (Italy)	46.42	10.62	2010-2011	2650-3769	7.94	784	Carturan et al. (2015)
Tsanteleina (Italy)	45.48	7.06	2015	2800-3445	13.76	805	Shaw et al., (2017)
Arolla (Switzerland)	45.97	7.52	2010	2550-3520	7.28	1663	Ayala et al. (2015)
McCall (USA)	69.21	-143.85	2004-2014	1375-2365	-2.28	500	Trolder et al. (2020)
Juncal Norte (Chile)	-33.01	-70.09	2007-2008	2900-5910	6.58	352	Ayala et al. (2015)
Greve (Chile)	-48.88	-73.52	2015-2016	0-2400	-0.1	12000	Bravo et al. (2019)
Pasterze (Austria)	47.09	12.71	1994	2150-3465	12.66	2761	Greuell and Böhm, (1998)
Universidad (Chile)	-34.69	-70.33	2009-2010	2463-4543	8.24	474	Bravo et al. (2017)
Peyto (Canada)	51.66	-116.55	2011	2260-3000	2.94	800	Pradhananga et al. (2020)*
Djankuat (Russia)	43.20	42.77	2017	3210-4000	12.13	950	Rets et al. (2019)

1206
1207
1208

*paper not yet submitted

Table 3. The coefficients of the original SM10 model and those fit to the k1 and k2 sensitivities on the Parlung glaciers and all glaciers where no warming effect was evident (see Figure 10).

Model	$k_1 = \beta_1 * \exp(\beta_2 * DF)$	$k_2 = \beta_3 + \beta_4 * \exp(-\beta_5 * DF)$
CMBC (Shea and Moore, 2010)	$\beta_1 = 0.977$ $\beta_2 = -4.4e-5$	$\beta_3 = 0.29$ $\beta_4 = 0.71$ $\beta_5 = 5.6e-4$
Parlung	$\beta_1 = 0.894 (0.805, 0.982)$ $\beta_2 = 2.972e-5 (-5.543e-5, 4.0e-6)$	$\beta_3 = 0.349 (0.241, 0.456)$ $\beta_4 = 0.624 (0.492, 0.757)$ $\beta_5 = 4.4e-3 (1.7e-4, 7.2e-4)$
All (no increased sensitivity on glacier terminus)	$\beta_1 = 0.923 (0.886, 0.96)$ $\beta_2 = 3.375e-5 (-5.543e-5, 4.0e-6)$	$\beta_3 = 0.343 (0.225, 0.46)$ $\beta_4 = 0.511 (0.38, 0.642)$ $\beta_5 = 4.2e-3 (1.5e-4, 6.9e-4)$

1209
1210
1211
1212
1213
1214